Chapter 12

Neutrino Scattering from Hadrons: Inelastic Scattering (II)

12.1 Introduction

The study of the various inelastic processes induced by photons, electrons, pions, and (anti) neutrinos from nucleons is very important as it provides information about the excitation mechanism of nucleons. This enables us to investigate the structure of nucleons as a composite of quarks and the role of gluons in the quark–quark forces using quantum chromodynamics (QCD). The inelastic processes induced by (anti)neutrinos are a unique source to determine the axial vector aspects of the nucleon structure and relate it to the pion physics. Moreover, in recent years, inelastic reactions induced by (anti)neutrinos leading to the production of mesons like pions, kaons, and ηs have become more relevant in the search for proton decay and for neutrino oscillations.

Within the standard model, proton stability is associated with baryon number conservation, as the proton being the lightest baryon, cannot decay into any other baryon when it is in the free state. It is believed that the baryon number conservation law is not a fundamental law; and there are models of grand unified theory (GUT) [503], which predict the lifetime of the proton to be of the order of 10^{31} years. To estimate a proton's lifetime, some calculations have also been performed using supersymmetry (SUSY) GUTs like SUSY SU(5) and SUSY SO(10). Generally, SUSY GUT models favor kaons (K^0 or K^+) in the final state if a proton decays. However, some of these models also predict decay modes where an eta meson is produced in the final state [504]. In the minimal SU(5) GUT, the predicted proton lifetime and decay to $e^+\pi^0$ is $10^{31\pm1}$ years, which has been ruled out by IMB [505], Kamiokande [506, 507], and Super-Kamiokande [508]. Although these experiments have not observed any event for the decay $p \rightarrow e^+\pi^0$, they have provided the limit for the proton's lifetime to be $10^{33\pm1}$ years. The best limit on the proton's lifetime comes from Super-Kamiokande [509] for the channel $p \rightarrow \nu K^+ > 5.9 \times 10^{33}$ years. Soudan-2 [510] looked for eta in the final state in the proton

https://doi.org/10.1017/9781108489065.013 Published online by Cambridge University Press

decay searches and found the best limit for the channels $p \to \mu^+\eta$ and $p \to e^+\eta$ to be 8.9×10^{31} years and 8.1×10^{31} years, respectively.

The search for proton decay had been going on for a long time in the deep underground experiment at the Kolar Gold Field (KGF) mines in India and simultaneously in the Homestake mines in South Dakota, which were started to study atmospheric neutrinos. No evidence has ever been found for proton decay but the best limits given by KGF and Homestake mines are 9×10^{30} years and $\sim 10^{31}$ years, respectively. In all these experiments of proton decay searches, atmospheric neutrino induced meson production is a significant part of the background. Therefore, it is important to estimate the cross sections for the neutrino interactions off the nucleon target in the few GeV energy region beyond the center of mass (CM) energy, $W > 1.2$ GeV, where inelastic processes are significant.

In the case of neutrino oscillation experiments, the inelastic production of pions is a major source of background through the decay of pions in charged leptons and photons. In the analysis of these experiments, the signature of oscillations depends on the yield of charged leptons like $\mu^{\mp}$, which are identified by their tracks and $e^{\mp}$ which are identified by the Bremsstrahlung photons produced by $e^{\mp}$. In the presence of inelastic channels, the produced $\pi^{\pm}$s decay into $\mu^{\pm}$ and the π^0s decay into two photons, which add to the background of genuine charged lepton production in the analysis of neutrino oscillation experiments. A similar situation arises at higher energies, that is, $E_{\nu/\bar{\nu}} \geq 1$ GeV where kaons and η mesons are also produced. In view of these considerations, the inelastic production of pions, kaons, and η mesons have become very important. In the following sections, we will study the production of single pions, kaons, and eta mesons and the associated production of kaons.

12.2 Single Pion Production

The various possible reactions which contribute to the single pion production induced by (anti)neutrinos on a nucleon target through charged current(CC) induced processes are the following:

$$\begin{aligned}
&\nu_l(k) + p(p) \to l^-(k') + p(p') + \pi^+(k_\pi) \qquad && \bar{\nu}_l(k) + n(p) \to l^+(k') + n(p') + \pi^-(k_\pi) \\
&\nu_l(k) + n(p) \to l^-(k') + n(p') + \pi^+(k_\pi) && \bar{\nu}_l(k) + p(p) \to l^+(k') + p(p') + \pi^-(k_\pi) \\
&\nu_l(k) + n(p) \to l^-(k') + p(p') + \pi^0(k_\pi) && \bar{\nu}_l(k) + p(p) \to l^+(k') + n(p') + \pi^0(k_\pi).
\end{aligned} \tag{12.1}$$

The neutral current(NC) induced processes are:

$$\begin{aligned}
&\nu_l(k) + p(p) \to \nu_l(k') + n(p') + \pi^+(k_\pi) \qquad && \bar{\nu}_l(k) + p(p) \to \bar{\nu}_l(k') + p(p') + \pi^0(k_\pi) \\
&\nu_l(k) + p(p) \to \nu_l(k') + p(p') + \pi^0(k_\pi) && \bar{\nu}_l(k) + p(p) \to \bar{\nu}_l(k') + n(p') + \pi^+(k_\pi) \\
&\nu_l(k) + n(p) \to \nu_l(k') + n(p') + \pi^0(k_\pi) && \bar{\nu}_l(k) + n(p) \to \bar{\nu}_l(k') + n(p') + \pi^0(k_\pi) \\
&\nu_l(k) + n(p) \to \nu_l(k') + p(p') + \pi^-(k_\pi) && \bar{\nu}_l(k) + n(p) \to \bar{\nu}_l(k') + p(p') + \pi^-(k_\pi),
\end{aligned} \tag{12.2}$$

https://doi.org/10.1017/9781108489065.013 Published online by Cambridge University Press

where $l = e, \mu, \tau$. The quantities in the parentheses represent the four momenta of the corresponding particles.

Single pion production induced by neutrinos and antineutrinos was the first inelastic process to be studied in detail using the methods for analyzing photo- and electro- production of pions induced by electromagnetic currents which are vector currents. The weak vector current contribution to (anti)neutrino induced pion production is obtained in terms of the amplitudes of the electroproduction of pions assuming the hypothesis of conserved vector current (CVC). In the case of axial vector current, the hypothesis of the partially conserved axial vector current (PCAC) and other symmetry properties of the axial vector current are used to calculate its contribution to the inelastic pion production.

Various methods have been used in the last 50 years to calculate the single pion production such as the dynamical model with dispersion relations [462, 463, 464, 294, 465, 466, 511, 512], quark models with higher symmetry [471, 513, 492, 514, 515, 516], phenomenological Lagrangians [473, 517, 518], and effective Lagrangians based on the chiral symmetry [481, 482, 483, 485, 484, 487]. In the following, we illustrate the salient features of the method based on the effective Lagrangian with chiral symmetry which has been outlined in Chapter 11, to calculate the processes shown in Eqs. (12.1) and (12.2) and extend it to SU(3) to describe the production of kaons and η particles.

In the following sections, charged and neutral current induced single pion production on a free nucleon target is discussed. The contribution of the non-resonant background terms and contributions from the spin $1/2$ and $3/2$ resonances excitations are discussed separately.

12.2.1 Charged current

The differential scattering cross section for the charged current induced process mentioned in Eq. (12.1), may be written as

$$d\sigma = \frac{1}{4(2\pi)^5 k\cdot p}\frac{d\vec{k}'}{(2E')}\frac{d\vec{p}\,'}{(2E'_p)}\frac{d\vec{p}_m}{(2E_m)}\delta^4(k+p-k'-p'-k_\pi)\overline{\sum}\sum|\mathcal{M}|^2, \quad (12.3)$$

where E', E'_p represent the energy of the outgoing lepton and nucleon, respectively and M is the nucleon mass. In the case of pion production, $E_m = E_\pi$ and $\vec{p}_m = \vec{p}_\pi$, where E_π and $\vec{p}_\pi$, respectively, are the energy and three-momentum of the outgoing pion. $\overline{\sum}\sum|\mathcal{M}|^2$ is the square of the transition amplitude averaged (summed) over the spins of the initial (final) state. The transition amplitude is expressed as

$$\mathcal{M} = \frac{G_F}{\sqrt{2}}\cos\theta_C\, l_\mu j^\mu, \quad (12.4)$$

where θ_C is the Cabibbo angle, l_μ and j^μ are the leptonic and hadronic currents, respectively, and G_F is the Fermi coupling constant. The weak leptonic current is written as

$$l_\mu = \bar{u}(k')\gamma_\mu(1\mp\gamma_5)u(k), \quad (12.5)$$

https://doi.org/10.1017/9781108489065.013 Published online by Cambridge University Press

where negative (positive) sign is for the (anti)neutrino induced processes. j^μ describes the total hadronic matrix element for the $W^\pm + N \rightarrow N' + \pi$ interaction for which both the non-resonant background terms and the resonance excitations followed by their decay to $N\pi$ contribute; they are obtained using an effective Lagrangian for $W^i + N \rightarrow N' + \pi$ interactions. The Feynman diagrams which may contribute to the matrix element of the hadronic current are shown in Figure 12.1. The non-resonant background terms include five diagrams viz., direct nucleon pole (NP), cross nucleon pole (CP), contact term (CT), pion pole (PP), and pion in flight (PF) terms. For $P_{33}(1232)$ resonance, we have included both direct (s channel) and cross (u channel) diagrams. Apart from the $P_{33}(1232)$ resonance, we have also included contributions from $P_{11}(1440)$, $S_{11}(1535)$ and, $S_{11}(1650)$ spin half resonances and $D_{13}(1520)$ and $P_{13}(1720)$ spin 3/2 resonances and considered both s channel and u channel contributions. In the following sections, we will write the matrix elements for the non-resonant diagrams using the chiral Lagrangian given in Eqs. (11.220)–(11.226) and for the resonance excitations and their subsequent decay using the formalism given in Chapter 11.

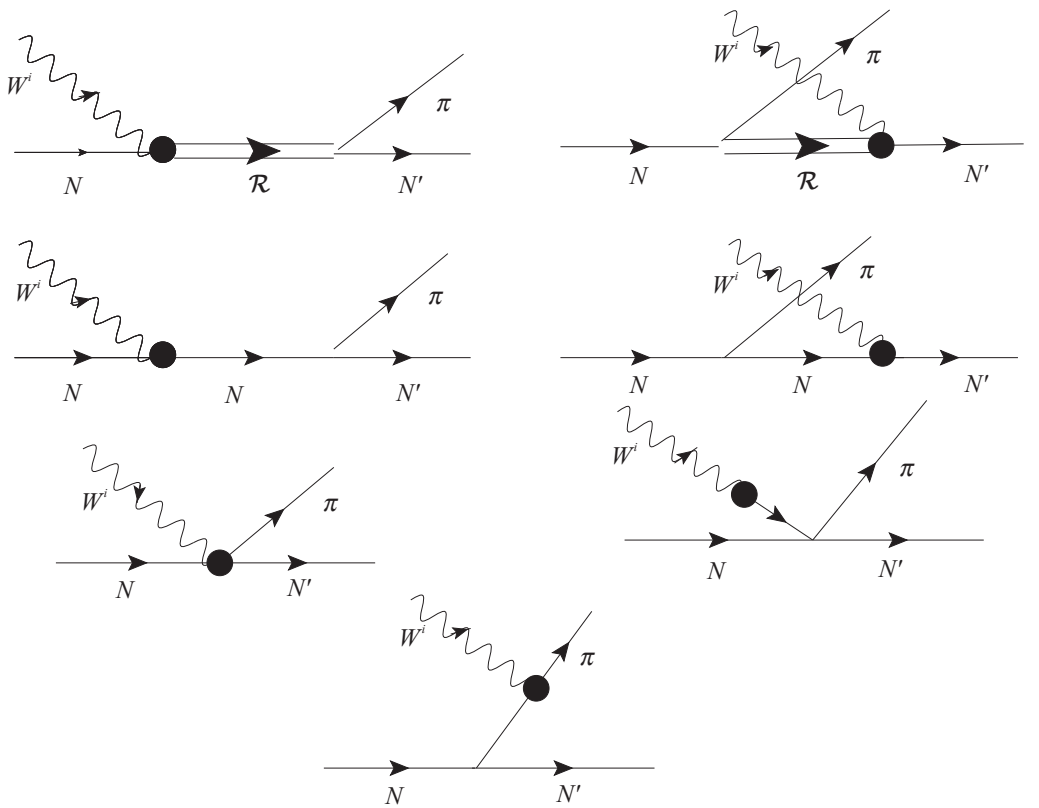

Figure 12.1 Feynman diagrams contributing for the process $W^i N \rightarrow N'\pi^{\pm,0}$, where $(W^i \equiv W^\pm\ ; i = \pm)$ for the charged current processes and $(W^i \equiv Z^0\ ; i = 0)$ for the neutral current processes with $N, N' = p$ or n. The first row represents the direct and cross diagrams for the resonance production where R stands for the different resonances. The second row represents the nucleon and cross nucleon terms. The contact and pion pole terms are shown in the third row and the last row represents the pion in flight terms.

https://doi.org/10.1017/9781108489065.013 Published online by Cambridge University Press

Non-resonant background contribution

The contribution from the non-resonant background terms may be obtained using the non-linear sigma model discussed in Chapter 11. They are expressed as [481]

$$
\begin{aligned}
j^{\mu}\big|_{NP} &= \mathcal{A}^{NP}\bar{u}(p')\not{k}_{\pi}\gamma_5\frac{\not{p}+\not{q}+M}{(p+q)^2-M^2+i\epsilon}\left[V_N^{\mu}(q^2)-A_N^{\mu}(q^2)\right]u(p),\\
j^{\mu}\big|_{CP} &= \mathcal{A}^{CP}\bar{u}(p')\left[V_N^{\mu}(q^2)-A_N^{\mu}(q^2)\right]\frac{\not{p}'-\not{q}+M}{(p'-q)^2-M^2+i\epsilon}\not{k}_{\pi}\gamma_5 u(p),\\
j^{\mu}\big|_{CT} &= \mathcal{A}^{CT}\bar{u}(p')\gamma^{\mu}\left(g_1 f_{CT}^{V}(q^2)\gamma_5-f_{\rho}\left((q-k_{\pi})^2\right)\right)u(p),\\
j^{\mu}\big|_{PP} &= \mathcal{A}^{PP}f_{\rho}\left((q-k_{\pi})^2\right)\frac{q^{\mu}}{m_{\pi}^2-q^2}\bar{u}(p')\not{q}\,u(p),\\
j^{\mu}\big|_{PF} &= \mathcal{A}^{PF}f_{PF}(q^2)\frac{(2k_{\pi}-q)^{\mu}}{(k_{\pi}-q)^2-m_{\pi}^2}2M\bar{u}(p')\gamma_5 u(p),
\end{aligned}
\tag{12.6}
$$

where $q(=k-k')$ is the four-momentum transfer and m_{π} is the mass of pion. The constant factor $\mathcal{A}^i, i =$ NP, CP, CT, PP, and PF, are tabulated in Table 12.1.

Table 12.1 The values of constant term ($\mathcal{A}^i$) appearing in Eq. (12.6), where i corresponds to the nucleon pole (NP), cross nucleon pole (CP), contact term (CT), pion pole (PP), and pion in flight (PF) terms. f_{π} is the pion weak decay constant and $g_A = g_1$ is nucleon axial vector coupling.

Constant term →	$\mathcal{A}$(CC ν)			$\mathcal{A}$(CC $\bar{\nu}$)			$\mathcal{A}$(NC $\nu(\bar{\nu})$)			
Final states →	$p\pi^+$	$n\pi^+$	$p\pi^0$	$n\pi^-$	$n\pi^0$	$p\pi^-$	$n\pi^+$	$p\pi^0$	$p\pi^-$	$n\pi^0$
NP	0	$\frac{-ig_1}{\sqrt{2}f_{\pi}}$	$\frac{-ig_1}{2f_{\pi}}$	0	$\frac{ig_1}{2f_{\pi}}$	$\frac{-ig_1}{\sqrt{2}f_{\pi}}$	$\frac{-ig_1}{\sqrt{2}f_{\pi}}$	$\frac{-ig_1}{2f_{\pi}}$	$\frac{ig_1}{\sqrt{2}f_{\pi}}$	$\frac{-ig_1}{2f_{\pi}}$
CP	$\frac{-ig_1}{\sqrt{2}f_{\pi}}$	0	$\frac{ig_1}{2f_{\pi}}$	$\frac{-ig_1}{\sqrt{2}f_{\pi}}$	$\frac{-ig_1}{2f_{\pi}}$	0	$\frac{ig_1}{\sqrt{2}f_{\pi}}$	$\frac{-ig_1}{2f_{\pi}}$	$\frac{-ig_1}{\sqrt{2}f_{\pi}}$	$\frac{-ig_1}{2f_{\pi}}$
CT	$\frac{-i}{\sqrt{2}f_{\pi}}$	$\frac{i}{\sqrt{2}f_{\pi}}$	$\frac{i}{f_{\pi}}$	$\frac{-i}{\sqrt{2}f_{\pi}}$	$\frac{-i}{f_{\pi}}$	$\frac{i}{\sqrt{2}f_{\pi}}$	$\frac{\sqrt{2}i}{f_{\pi}}$	0	$\frac{-\sqrt{2}i}{f_{\pi}}$	0
PP	$\frac{i}{\sqrt{2}f_{\pi}}$	$\frac{-i}{\sqrt{2}f_{\pi}}$	$\frac{-i}{f_{\pi}}$	$\frac{i}{\sqrt{2}f_{\pi}}$	$\frac{i}{f_{\pi}}$	$\frac{-i}{\sqrt{2}f_{\pi}}$	$\frac{-\sqrt{2}i}{f_{\pi}}$	0	$\frac{\sqrt{2}i}{f_{\pi}}$	0
PF	$\frac{-ig_1}{\sqrt{2}f_{\pi}}$	$\frac{ig_1}{\sqrt{2}f_{\pi}}$	$\frac{ig_1}{f_{\pi}}$	$\frac{-ig_1}{\sqrt{2}f_{\pi}}$	$\frac{-ig_1}{f_{\pi}}$	$\frac{ig_1}{\sqrt{2}f_{\pi}}$	$\frac{\sqrt{2}ig_1}{f_{\pi}}$	0	$\frac{-\sqrt{2}ig_1}{f_{\pi}}$	0

The vector $(V_N^{\mu}(q^2))$ and axial vector $(A_N^{\mu}(q^2))$ currents for the NP and CP diagrams are calculated neglecting the second class currents and are given by:

$$V_N^{\mu}(q^2) = f_1(q^2)\gamma^{\mu}+f_2(q^2)i\sigma^{\mu\nu}\frac{q_{\nu}}{2M}, \tag{12.7}$$

$$A_N^{\mu}(q^2) = \left(g_1(q^2)\gamma^{\mu}+g_3(q^2)\frac{q^{\mu}}{M}\right)\gamma^5, \tag{12.8}$$

where $f_{1,2}(q^2)$ and $g_{1,3}(q^2)$ are the vector and axial vector form factors for the nucleons. The isovector form factors viz. $f_{1,2}(q^2)$ are expressed as:

$$f_{1,2}(q^2) = F_{1,2}^{p}(q^2)-F_{1,2}^{n}(q^2), \tag{12.9}$$

https://doi.org/10.1017/9781108489065.013 Published online by Cambridge University Press

where $F_i^{p,n}(q^2)$; $i = 1, 2$ are the Dirac-Pauli form factors of nucleons. These form factors are, in turn, expressed in terms of the experimentally determined Sachs electric $G_E^{p,n}(q^2)$ and magnetic $G_M^{p,n}(q^2)$ form factors [414], which have been discussed in Chapter 10.

The axial vector form factor $(g_1(q^2))$ is generally taken to be of dipole form and is given by

$$g_1(q^2) = g_A(0) \left[1 - \frac{q^2}{M_A^2}\right]^{-2}, \tag{12.10}$$

where the values of $g_A(0)$ and M_A are quoted in Chapter 10.

The pseudoscalar form factor $g_3(q^2)$ is related to $g_1(q^2)$, assuming PCAC and the pion pole dominance, through the relation

$$g_3(q^2) = \frac{2M^2\, g_1(q^2)}{m_\pi^2 - q^2}. \tag{12.11}$$

In order to conserve vector current at the weak vertex, the two form factors viz. $f_{PF}(q^2)$ and $f_{CT}^V(q^2)$ are expressed in terms of the isovector nucleon form factor as [481]

$$f_{PF}(q^2) = f_{CT}^V(q^2) = 2f_1^V(q^2). \tag{12.12}$$

The form factor $(f_\rho(q^2))$ is taken to be of the monopole form [481]:

$$f_\rho(q^2) = \frac{1}{1 - q^2/m_\rho^2}; \qquad \text{with} \qquad m_\rho = 0.776 \text{ GeV}. \tag{12.13}$$

In order to be consistent with the assumption of PCAC, $f_\rho(q^2)$ has also been used with the axial vector part of the contact term.

Resonance contribution

The basic (anti)neutrino induced reactions for pion production through resonance excitations are the following:

$$\nu_l(k) + N(p) \to l^-(k') + R(p_R) \hookrightarrow N'(p') + \pi(k_\pi), \tag{12.14}$$

$$\bar{\nu}_l(k) + N(p) \to l^+(k') + R(p_R) \hookrightarrow N'(p') + \pi(k_\pi), \tag{12.15}$$

where R stands for any resonance which contributes to the pion production. In the next section, we demonstrate by including the different positive and negative parity, spin $1/2$ and $3/2$ resonances. We have included six resonances, viz., $P_{33}(1232)$, $P_{11}(1440)$, $D_{13}(1520)$,

https://doi.org/10.1017/9781108489065.013 Published online by Cambridge University Press

$S_{11}(1535)$, $S_{11}(1650)$, and $P_{13}(1720)$. However, it may be generalized to any set of resonances with the same parity and spin. The resonances which have been considered here for demonstration are summarized in Tables 11.1 and 11.2 of Chapter 11 with their properties like mass, decay width, etc. We write the matrix elements for the resonance excitations for spin $1/2$ and $3/2$ resonances using the matrix element for the purely weak excitation $\nu N \to l^- R_{\frac{1}{2}(\frac{3}{2})}$ given in Eqs. (11.2) and (11.76) and the matrix elements for the strong decay process $R_{\frac{1}{2}(\frac{3}{2})} \to N\pi$ using the Lagrangian given in Eqs. (11.34) and (11.89) for spin $1/2$ ($R_{\frac{1}{2}}$) and spin $3/2$ ($R_{\frac{3}{2}}$) resonances.

(i) Spin $\frac{1}{2}$ resonances

In Chapter 11, we have already discussed in detail resonance excitation, where the matrix element, vector and axial vector hadronic form factors, and their determination by the assumption of CVC and PCAC hypotheses are explained. Using the inputs from Chapter 11, the most general form of the hadronic currents for the s channel (direct diagram) and u channel (cross diagram) processes, shown in Figure 12.1, where a resonant state $R_{1/2}$ is produced and decays to a pion in the final state, are written as

$$j^\mu\big|^{\frac{1}{2}}_{R} = i\,\mathcal{C}^{\mathcal{R}}\bar{u}(p')\not{k}_\pi\Gamma\frac{\not{p}+\not{q}+M_R}{(p+q)^2-M_R^2+iM_R\Gamma_R}\Gamma^\mu_{\frac{1}{2}}u(p), \tag{12.16}$$

$$j^\mu\big|^{\frac{1}{2}}_{CR} = i\,\mathcal{C}^{\mathcal{R}}\bar{u}(p')\Gamma^\mu_{\frac{1}{2}}\frac{\not{p}'-\not{q}+M_R}{(p'-q)^2-M_R^2+iM_R\Gamma_R}\not{k}_\pi\Gamma u(p), \tag{12.17}$$

where M_R and Γ_R represent the mass and decay width of the resonance, respectively. $\Gamma = 1\ (\gamma_5)$ for the positive (negative) parity resonances, $\Gamma^\mu_{1/2}$ for the positive (negative) parity resonances are defined in Chapter 11 (Eqs. (11.5) and (11.6)), and $\mathcal{C}^{\mathcal{R}}$ is a constant which includes the coupling strength in terms of f_π, isopin factor involved in $R_{1/2} \to N\pi$ transition, etc. The constant $\mathcal{C}^{\mathcal{R}}$ for the various channels have been tabulated in Table 12.2. The formalism for determining the coupling strength, $f_{NR_{1/2}\pi}$ for the $R_{1/2} \to N\pi$ transitions in terms of the decay width has already been discussed in Chapter 11.

(ii) Spin $\frac{3}{2}$ resonances

The matrix element as well as the vector and axial vector transition form factors for the spin $3/2$ resonances were discussed in Chapter 11. One may write the most general form of the hadronic current for the s channel (direct diagram) and u channel (cross diagram) processes where a resonant state $R_{3/2}$ is produced and decays to a pion in the final state as

$$j^\mu\big|^{\frac{3}{2}}_{R} = i\,\mathcal{C}^{\mathcal{R}}\bar{u}(p')k^\alpha_\pi\Gamma\frac{\not{p}_R+M_R}{p_R^2-M_R^2+iM_R\Gamma_R}\mathcal{P}_{\alpha\beta}(p_R)\Gamma^{\beta\mu}_{\frac{3}{2}}(p,q)u(p),\ p_R = p+q, \tag{12.18}$$

$$j^\mu\big|^{\frac{3}{2}}_{CR} = i\,\mathcal{C}^{\mathcal{R}}\bar{u}(p')\hat{\Gamma}^{\mu\alpha}_{\frac{3}{2}}(p',-q)\frac{\not{p}_R+M_R}{p_R^2-M_R^2+iM_R\Gamma_R}P^{3/2}_{\alpha\beta}(p_R)k^\beta_\pi\Gamma u(p),\ p_R = p'-q. \tag{12.19}$$

In Eqs. (12.18) and (12.19), $\Gamma = 1\ (\gamma_5)$ is for the positive (negative) parity resonances, $\hat{\Gamma}^{\mu\alpha}_{\frac{3}{2}} = \gamma_0\Gamma^{\mu\alpha\dagger}_{\frac{3}{2}}\gamma_0$. The projector operator $P^{3/2}_{\alpha\beta}(p_R)$ and $\Gamma^{\mu\nu}_{\frac{3}{2}}$ for the positive (negative) parity

https://doi.org/10.1017/9781108489065.013 Published online by Cambridge University Press

resonances are defined in Chapter 11. $\mathcal{C}^{\mathcal{R}}$ is the coupling for the $R_{3/2} \to N\pi$ transitions and has been tabulated in Table 12.2. The coupling strength, $f_{NR_{3/2}\pi}$ for the $R_{3/2} \to N\pi$ transitions in terms of the decay width have already been discussed in Chapter 11.

Table 12.2 Coupling constant ($\mathcal{C}^{\mathcal{R}}$) for spin $\frac{1}{2}$ and spin $\frac{3}{2}$ resonances in the case of charged current induced processes. Here, $f^\star$ stands for $R_{1/2} \to N\pi$ coupling which for $\Delta(1232)$ resonance is $f_{N\Delta\pi}$ and is $f_{NR_{1/2}\pi}(f_{NR_{3/2}\pi})$ for spin $\frac{1}{2}(\frac{3}{2})$ resonances.

Process	$\mathcal{C}^{\mathcal{R}}$(CC ν)			$\mathcal{C}^{\mathcal{R}}$(CC $\bar{\nu}$)		
	$p\pi^+$	$n\pi^+$	$p\pi^0$	$n\pi^-$	$n\pi^0$	$p\pi^-$
$P_{33}(1232)$	$\frac{\sqrt{3}f^\star}{m_\pi}$	$\sqrt{\frac{1}{3}}\frac{f^\star}{m_\pi}$	$-\sqrt{\frac{2}{3}}\frac{f^\star}{m_\pi}$	$\frac{\sqrt{3}f^\star}{m_\pi}$	$\sqrt{\frac{2}{3}}\frac{f^\star}{m_\pi}$	$\sqrt{\frac{1}{3}}\frac{f^\star}{m_\pi}$
$P_{11}(1440)$	0	$\sqrt{2}\frac{f^\star}{m_\pi}$	$\frac{f^\star}{m_\pi}$	0	$-\frac{f^\star}{m_\pi}$	$\sqrt{2}\frac{f^\star}{m_\pi}$
$D_{13}(1520)$	0	$\sqrt{2}\frac{f^\star}{m_\pi}$	$\frac{f^\star}{m_\pi}$	0	$-\frac{f^\star}{m_\pi}$	$\sqrt{2}\frac{f^\star}{m_\pi}$
$S_{11}(1535)$	0	$\sqrt{2}\frac{f^\star}{m_\pi}$	$\frac{f^\star}{m_\pi}$	0	$-\frac{f^\star}{m_\pi}$	$\sqrt{2}\frac{f^\star}{m_\pi}$
$S_{11}(1650)$	0	$\sqrt{2}\frac{f^\star}{m_\pi}$	$\frac{f^\star}{m_\pi}$	0	$-\frac{f^\star}{m_\pi}$	$\sqrt{2}\frac{f^\star}{m_\pi}$
$P_{13}(1720)$	0	$\sqrt{2}\frac{f^\star}{m_\pi}$	$\frac{f^\star}{m_\pi}$	0	$-\frac{f^\star}{m_\pi}$	$\sqrt{2}\frac{f^\star}{m_\pi}$

12.2.2 Neutral current

In this section, we will briefly discuss the single pion production induced by neutral currents. The differential scattering cross section for the neutral current induced process mentioned in Eq. (12.2) is given in Eq. (12.3). The transition amplitude is expressed as

$$\mathcal{M} = \frac{G_F}{\sqrt{2}}\, l_\mu j^\mu, \tag{12.20}$$

where the weak leptonic current is given in Eq. (12.5). j^μ describes the total hadronic matrix element for the neutral current induced pion production; both the non-resonant background terms and the resonance excitation followed by their decay in $N\pi$ contribute. The same analogy as we have done for the charged current induced pion production to obtain the non-resonant and resonant contributions is followed.

In the following sections, we present the formalism in brief which can be used for the non-resonant background terms and the resonant contributions to the single pion production processes in the neutral current sector.

Non-resonant background contribution

The contribution from the non-resonant background terms in the case of neutral current induced reactions $ZN \to N'\pi$ is obtained using the non-linear sigma model. The hadronic currents for the different diagrams presented in Figure 12.1 are given in Eq. (12.6) with the values of the constants $\mathcal{A}^i$ tabulated in Table 12.1.

https://doi.org/10.1017/9781108489065.013 Published online by Cambridge University Press

In the absence of second class currents, the vector $(V_N^\mu(q^2))$ and the axial vector $(A_N^\mu(q^2))$ currents for the neutral current induced nucleon pole diagrams are given by,

$$V_N^\mu(q^2) = \tilde{f}_1(q^2)\gamma^\mu + \tilde{f}_2(q^2)i\sigma^{\mu\nu}\frac{q_\nu}{2M}, \tag{12.21}$$

$$A_N^\mu(q^2) = \left(\tilde{g}_1(q^2)\gamma^\mu + \tilde{g}_3(q^2)\frac{q^\mu}{M}\right)\gamma^5, \tag{12.22}$$

where $\tilde{f}_{1,2}(q^2)$ and $\tilde{g}_{1,3}(q^2)$ are the vector and axial vector neutral current form factors for the nucleons. The vector form factors are expressed as:

$$\tilde{f}_{1,2}(q^2) \xrightarrow{\text{for p}} \tilde{f}_{1,2}^p(q^2) = \left(\frac{1}{2} - 2\sin^2\theta_W\right)F_{1,2}^p(q^2) - \frac{1}{2}F_{1,2}^n(q^2), \tag{12.23}$$

$$\tilde{f}_{1,2}(q^2) \xrightarrow{\text{for n}} \tilde{f}_{1,2}^n(q^2) = \left(\frac{1}{2} - 2\sin^2\theta_W\right)F_{1,2}^n(q^2) - \frac{1}{2}F_{1,2}^p(q^2). \tag{12.24}$$

where θ_W is the Weinberg angle (Chapter 8). $F_{1,2}^p$ and $F_{1,2}^p$ are the Dirac-Pauli form factors of the nucleon (Chapter 10). On the other hand, the axial vector form factor$(\tilde{g}_1(q^2))$ is given by

$$\tilde{g}_1(q^2) = \tilde{g}_1^{p,n}(0)\left[1 - \frac{q^2}{M_A^2}\right]^{-2}, \tag{12.25}$$

with $\tilde{g}_1^{p,n}(q^2) = \pm\frac{1}{2}g_1(q^2)$, where the plus (minus) sign stands for a proton (neutron) target. The contribution of the pseudoscalar form factor $\tilde{f}_P(q^2)$ vanishes for the neutral current processes as its contribution is proportional to the lepton mass.

The form factors $f_{PF}(q^2)$ and $f_{CT}^V(q^2)$ in the neutral current interaction becomes $\tilde{f}_{PF}(q^2)$ and $\tilde{f}_{CT}^V(q^2)$ and transforms in the same way as the nucleon pole vector form factors do. Thus,

$$\tilde{f}_{PF}(q^2) = \tilde{f}_{CT}^V(q^2) = 2\tilde{f}_1(q^2), \tag{12.26}$$

with $\tilde{f}_1(q^2)$ for the neutral current induced proton and neutron processes given in Eqs. (12.23) and (12.24), respectively. However, the parameterization of f_ρ remains the same as in the case of charged current induced processes given in Eq. (12.13). It can be seen from Table 12.2 that not all the terms contribute in the case of neutral currents (NC) production of π^0 mesons. In all the cases, the contribution from the isoscalar currents arising from the strangeness content of the nucleon are neglected.

Resonant contribution

The basic (anti)neutrino induced reactions for the pion production through the resonance excitations in the neutral current sector are the following:

https://doi.org/10.1017/9781108489065.013 Published online by Cambridge University Press

$$\nu_l(\bar{\nu}_l)(k) + N(p) \to \nu_l(\bar{\nu}_l)(k') + R(p_R).$$
$$\hookrightarrow N'(p') + \pi(k_\pi). \tag{12.27}$$

In the following, we will discuss spin 1/2 and 3/2 resonance excitations and their subsequent decay in $N\pi$.

(i) Spin $\frac{1}{2}$ resonances

The general form of the charged hadronic currents for the s channel (direct diagram) and u channel (cross diagram) processes when a resonance $R_{1/2}$ is produced and the particle subsequently decays to a pion in the final state, are written in Eqs. (12.16) and (12.17), respectively with the constant $\mathcal{C}_{\mathcal{R}}$ given in Table 12.2. In the case of neutral currents (NC) induced pion production, the coefficients $\mathcal{C}_{\mathcal{R}}$ are also given in Table 12.2 for different channels. In the case of weak vertex, the vector form factors appearing in $\Gamma_{\frac{1}{2}}$ are expressed as Eq. (11.125) (Chapter 11) in the vector sector and Eq. (11.126) (Chapter 11), in the axial vector sector. It should be noted from the structure of the vector form factors in the weak neutral current that they depend explicitly on the mixing angle θ_W unlike the weak charged current form factors. We neglect here the strangeness content of the nucleons which would contribute through the strangeness form factors both in the vector and axial vector sectors.

(ii) Spin $\frac{3}{2}$ resonances

In this case also, the most general form of the charged hadronic current for the s channel (direct diagram) and u channel (cross diagram) processes in the case of neutral current induced processes, where a resonant state $R_{3/2}$ is produced and the particle decays to a pion in the final state is given in Eqs. (12.18) and (12.19), respectively. The vector and axial vector transition form factors has already been discussed in Eqs. (11.153) and (11.154) of Chapter 11.

12.2.3 Cross sections

The cross section for the inelastic production of pions is calculated using the matrix elements for the non-resonant and resonance diagrams given in Eqs. (12.6), (12.16), (12.17), (12.18), and (12.19). However, there is ambiguity regarding the phase between various diagrams shown in Figure 12.1, when adding the matrix elements. Since the non-resonant terms are obtained from the Lagrangian derived from the chiral symmetry, the phases are predicted uniquely as written in the equations. But there could be a phase between the non-resonant and the resonance diagrams which could, in principle, be different for each resonance R considered. In the calculations based on the quark model with higher symmetry, there is no ambiguity as the nucleons and higher resonances are predicted from the same model [494] but in the case of effective Lagrangians, the phase is arbitrary, that is, the total matrix element for the hadronic current J^μ is written as

$$\langle j^\mu \rangle = \langle j^\mu \rangle_{NR} + e^{i\phi_i} \langle j^\mu \rangle_{R_i}, \tag{12.28}$$

https://doi.org/10.1017/9781108489065.013 Published online by Cambridge University Press

where ϕ is the phase difference between the diagrams in the first row and the rest of the diagrams in Figure 12.1. However, we add them coherently, that is, $\phi = 0$ for the present purpose. A calculation done with $\phi_i = \pi$, $R_i = \Delta$ (neglecting other resonances) does not reproduce the experimental results [481]. A choice of $\phi_i = \pi/2$ for all i will give the incoherent sum of all the non-resonant and resonance contributions. Adding coherently $j^\mu_{R_i}$ is expressed as

$$j^\mu_{R_i} = j^\mu_{R_s} + j^\mu_{R_u}, \tag{12.29}$$

where R can be any resonance and the net contribution of these resonances, is written as

$$j^\mu_{R_i} = j^\mu_{P_{33}(1232)} + j^\mu_{P_{11}(1440)} + j^\mu_{S_{11}(1535)} + j^\mu_{S_{11}(1650)} + j^\mu_{D_{13}(1520)} + j^\mu_{P_{13}(1720)}, \tag{12.30}$$

with $i = s, u$. $j^\mu_{\rm NR}$ for the charged current induced processes is given by

$$j^\mu_{\rm NR} = j^\mu\big|_{NP} + j^\mu\big|_{CP} + j^\mu\big|_{CT} + j^\mu\big|_{PP} + j^\mu\big|_{PF}. \tag{12.31}$$

The cross section is then calculated using Eqs. (12.3), (12.4), and (12.28). The existing experimental data on the single pion production process from (almost) free nucleons are available only from the old bubble chamber experiments performed almost 40 years ago at ANL [458] and BNL [519] with deuteron and hydrogen targets. In view of this, the deuteron effects should also be taken into account.

The deuteron effect can be taken into account by writing the differential scattering cross section as

$$\left(\frac{d\sigma}{dQ^2dW}\right)_{\nu d} = \int d\vec{p}^{\,d}_p |\Psi_d(\vec{p}^{\,d}_p)|^2 \frac{M}{E^d_p}\left(\frac{d\sigma}{dQ^2dW}\right)_{\nu N}, \tag{12.32}$$

where $p^\mu = (E^d_p, \vec{p}^{\,d}_p)$ is the four-momentum of the proton bound inside the deuteron with $E^d_p (= M_D - \sqrt{M^2 + \vec{p}^{\,2}_n}, \vec{p}_n = -\vec{p}_D)$ as the energy of the off-shell proton inside the deuteron, M_D is the deuteron mass, and $\psi_d(\vec{p}^{\,d}_p)$ is the wave function of the deuteron [520].

The data available from ANL and BNL on $\nu_\mu p \to \mu^- p\pi^+$ differ with each other by about $30 - 40\%$ which has been attributed in the past to the different flux normalization in these experiments. These data, when used to fix various parameters of theoretical models of reaction mechanisms for the single pion production, give rise to considerable uncertainties in the determination of these parameters, which in turn, lead to higher uncertainties in predicting the single pion production cross section from the nuclear targets. Reanalysis of the old bubble chamber data give a consistent set of data from ANL [458] and BNL [519] experiments either by minimizing the neutrino flux uncertainties [521, 522] or by reconstructing the data using the cross section ratio for the single pion production to the quasielastic processes and observed quasielastic cross sections [523]. It is hoped that the use of reanalyzed/reconstructed data on free nucleon targets will help toward a better understanding of the pion production reaction mechanism. Nevertheless, the need for $\nu(\bar{\nu})$ experiments on free proton/deuteron targets with high statistics and precision is to be emphasized.

https://doi.org/10.1017/9781108489065.013 Published online by Cambridge University Press

In Figure 12.2, we show the results for the total scattering cross section for the process $\nu_\mu p \to \mu^- p\pi^+$. The results are presented in the $\Delta(1232)$ dominance model; the contributions from the non-resonant background terms are included. The results include the deuteron effect which was obtained using Eq. (12.32). It may be observed that the inclusion of the deuteron effect results in an overall reduction of $\sim 4-6\%$ in the total scattering cross section. The results are compared with the reanalyzed experimental data of ANL [458] and BNL [519] by Wilkinson et al. [523]. It may be noticed that due to the presence of the non-resonant background terms, there is an increase in the cross section which is about 12% at $E_{\nu_\mu} = 1$ GeV and becomes $\sim 8\%$ at $E_{\nu_\mu} = 2$ GeV. When a cut of $W \leq 1.4$ GeV or $W \leq 1.6$ GeV is applied, the increase in the total scattering cross section at $E_{\nu_\mu} = 1$ GeV is about 10% in both cases.

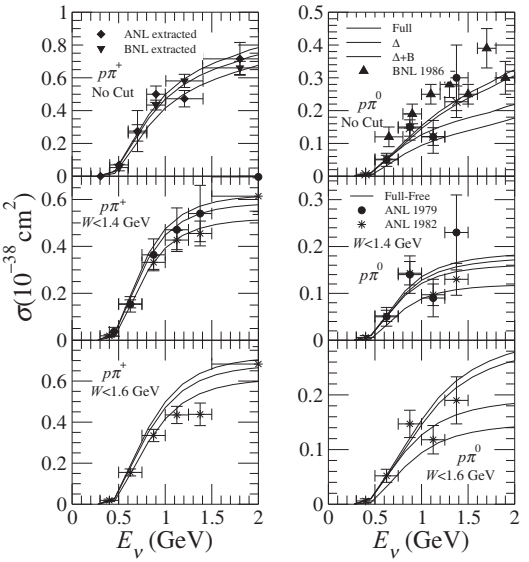

Figure 12.2 Total scattering cross section for the processes $\nu_\mu p \to \mu^- p\pi^+$ (left panel) and $\nu_\mu n \to \mu^- p\pi^0$ (right panel). The dashed line is the result calculated in the $\Delta(1232)$ dominance model, the dash-dotted line represents the result obtained when the non-resonant background terms are included. These two cases have the deuteron effect. The dotted line is the result of the full calculation without the deuteron effect while the solid line represents the results of the full model with the deuteron effect. The results in the top panel are obtained when no cut on the invariant mass is included. The middle (bottom) panel shows the results with a cut on the center of mass energy of 1.4 GeV (1.6 GeV). Diamond and down triangle represents the reanalyzed data of ANL and BNL by Wilkinson et al. [523]. Circle, star, and up triangle represent the original data from ANL [458] and BNL [519] experiments.

For the process $\nu_\mu + n \to \mu^- + p + \pi^0$, there are contributions from the non-resonant background terms as well as from the other higher resonance excitation terms besides the $\Delta(1232)$. The net contribution to the total pion production due to the presence of the non-resonant background terms in $\nu_\mu + n \to \mu^- + p + \pi^0$ reaction results in an increase in the cross section of about 26% at E_{ν_μ}=1 GeV which becomes 18% at E_{ν_μ}= 2 GeV. When other higher resonances are also taken into account, there is a further increase in the cross section by about 35% at E_{ν_μ}=1 GeV which becomes 40% at E_{ν_μ}= 2 GeV. Thus, we find that

https://doi.org/10.1017/9781108489065.013 Published online by Cambridge University Press

the inclusion of higher resonant terms leads to a significant increase in the cross section for the $\nu_\mu + n \rightarrow \mu^- + p + \pi^0$ process. Furthermore, it may also be concluded from these observations that with increase in neutrino energy, contributions from non-resonant background terms decrease while the total scattering cross section increases when the higher resonances are included. When a cut of $W \leq 1.4$GeV or $W \leq 1.6$GeV on the center of mass energy is applied, then the increase in the total scattering cross section at $E_{\nu_\mu} = 1$ GeV and 2 GeV is about 43% and 13%, respectively.

Figure 12.3 shows the total scattering cross section for the neutral current neutrino induced pion production processes. The experimental points are the data from the ANL experiment [524]. It may be observed that besides the $\Delta(1232)$ resonant term, there is significant contribution from the non-resonant background terms which results in an increase in the total scattering cross section in all the channels. Moreover, there is an $\sim 15\%$ enhancement in the cross sections in $\nu p \rightarrow \nu\pi^+ n$ and $\nu p \rightarrow \nu\pi^- p$ processes when higher resonant terms are included.

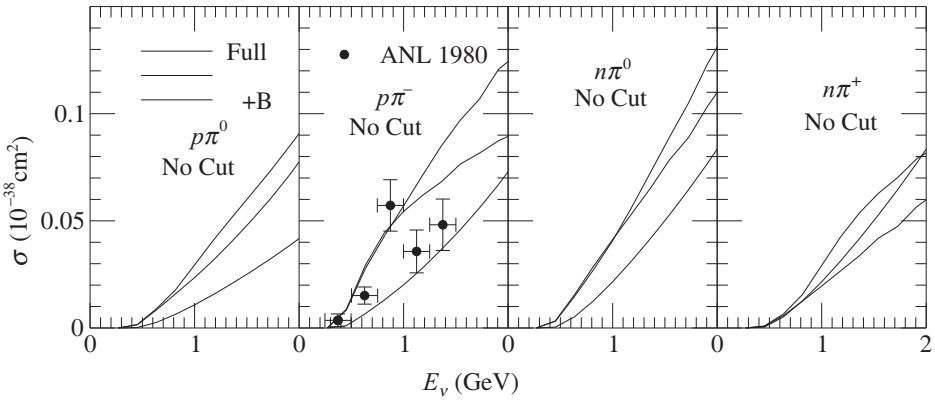

Figure 12.3 Total scattering cross section for neutral current neutrino induced pion production processes with deuteron effect and with no cut on W. The results presented from the left to the right panels are for $\nu p \rightarrow \nu p\pi^0$, $\nu n \rightarrow \nu p\pi^-$, $\nu n \rightarrow \nu n\pi^0$, and $\nu p \rightarrow \nu n\pi^+$ processes. Data points have been taken from ANL [524] experiment. Lines have the same meaning as in Fig. 12.2.

12.3 Eta Production

The (anti)neutrino induced eta production is interesting because of several reasons. Being an isoscalar particle, the η meson is an important probe that can be used to search for the strange quark content of nucleons [525]. A precise determination of the η production cross section would also help in understanding the background in the proton decay searches through the $p \rightarrow \eta e^+$ decays. Therefore, its background contribution due to the atmospheric neutrino interactions should be well estimated. Furthermore, η production is expected to be dominated by $S_{11}(1535)$ resonance excitation as this state appears near the threshold of the $N\eta$ system and has large branching ratio to η decay modes. A precise measurement of the cross section will also allow to determine the axial vector properties of this resonance.

https://doi.org/10.1017/9781108489065.013 Published online by Cambridge University Press

12.3.1 Charged current

In this section, we will discuss the weak production of η mesons via the charged current interactions. The channels that may contribute to the CC-η production (Figure12.4) are

$$\nu_\mu(k) + n(p) \longrightarrow \mu^-(k') + \eta(p_\eta) + p(p'), \tag{12.33}$$
$$\bar{\nu}_\mu(k) + p(p) \longrightarrow \mu^+(k') + \eta(p_\eta) + n(p'), \tag{12.34}$$

where the quantities in the parenthesis are the four-momenta of the particles.

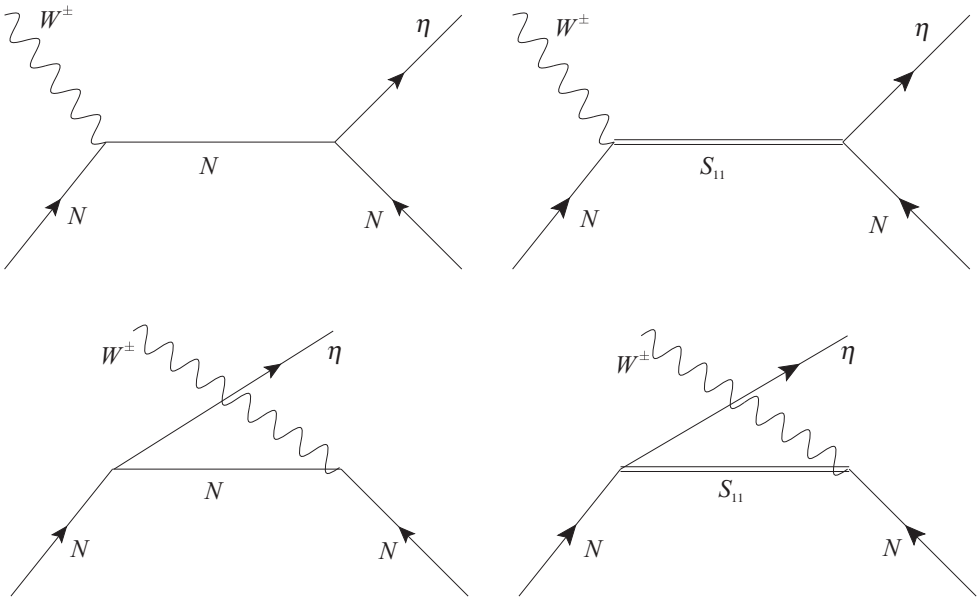

Figure 12.4 Feynman diagrams for the processes $\nu/\bar{\nu}(k) + N(p) \to \mu^\mp(k') + \eta(p_\eta) + N'(p')$. The first row from left to right: s channel nucleon pole (SC) and S_{11} resonance (SC N^*); the second row: u channel nucleon pole (UC) and S_{11} resonance (UC N^*).

The general expression of the differential scattering cross section for the reaction shown in Eqs. (12.33) and (12.34) in the laboratory frame is given in Eq. (12.3), with $\vec{p}_m = \vec{p}_\eta$ as the three-momentum of the outgoing eta meson and $E_m = E_\eta$, the energy of the eta meson. The transition matrix element, in terms of the leptonic and the hadronic currents, is given in Eq. (12.4). The leptonic current is given in Eq. (12.5); the hadronic current receives contributions from the non-resonant background terms as well as from the resonance excitations and their subsequent decay in $N\eta$.

Non-resonant background contribution

The hadronic currents for the non-resonant background terms, that is, Born diagrams (s and u channels) with nucleon poles, using the non-linear sigma model, is obtained as [488, 489],

$$J^\mu_{N(s)} = \frac{gV_{ud}}{2\sqrt{2}}\frac{D-3F}{2\sqrt{3}f_\pi}\bar{u}_N(p')\not{p}_\eta\gamma^5\frac{\not{p}+\not{q}+M}{(p+q)^2-M^2}\mathcal{O}^\mu_N u_N(p), \tag{12.35}$$

https://doi.org/10.1017/9781108489065.013 Published online by Cambridge University Press

$$J^{\mu}_{N(u)} = \frac{gV_{ud}}{2\sqrt{2}}\frac{D-3F}{2\sqrt{3}f_{\pi}}\bar{u}_N(p')\mathcal{O}^{\mu}_N\frac{\not{p}-\not{p}_{\eta}+M}{(p-p_{\eta})^2-M^2}\not{p}_{\eta}\gamma^5 u_N(p), \quad (12.36)$$

where

$$\mathcal{O}^{\mu}_N \equiv f_1(Q^2)\gamma^{\mu}+f_2(Q^2)i\sigma^{\mu\rho}\frac{q_{\rho}}{2M_N}-g_1(Q^2)\gamma^{\mu}\gamma^5-g_3(Q^2)\frac{q^{\mu}}{M}\gamma^5. \quad (12.37)$$

$f_{1,2}(q^2)$ are the isovector vector form factors and $g_{1,3}(q^2)$ are the axial vector and pseudoscalar form factors, respectively, for the nucleons; they are determined in the same manner as done in the case of pion production in Section 12.2.1.

Resonance contribution

For the resonant $S_{11}(1535)$ and $S_{11}(1650)$ channels, the hadronic currents are given by

$$J^{\mu}_{R(s)} = \frac{gV_{ud}}{2\sqrt{2}}ig_{\eta}\bar{u}_N(p')\not{p}_{\eta}\frac{\not{p}+\not{q}+M_R}{(p+q)^2-M_R^2+i\Gamma_R M_R}\mathcal{O}^{\mu}_R u_N(p), \quad (12.38)$$

$$J^{\mu}_{R(u)} = \frac{gV_{ud}}{2\sqrt{2}}ig_{\eta}\bar{u}_N(p')\mathcal{O}^{\mu}_R\frac{\not{p}-\not{p}_{\eta}+M_R}{(p-p_{\eta})^2-M_R^2+i\Gamma_R M_R}\not{p}_{\eta}u_N(p), \quad (12.39)$$

where

$$\mathcal{O}^{\mu}_R \equiv \frac{f_1(q^2)}{(2M)^2}(\not{q}q^{\mu}-q^2\gamma^{\mu})\gamma_5+\frac{f_2(q^2)}{2M}i\sigma^{\mu\rho}q_{\rho}\gamma_5-g_1(q^2)\gamma^{\mu}-\frac{g_3(q^2)}{M}q^{\mu}. \quad (12.40)$$

The determination of these vector and axial vector transition form factors were discussed in detail in Chapter 11.

The coupling g_{η} is determined in a similar manner as we have obtained $f_{NR\pi}$ in the case of pion production, but by substituting η in the place of π in the determination of the coupling presented in Chapter 11.

12.3.2 Neutral current

In this section, we will extend the formalism for the neutral current induced η production processes. The channels that contribute are given as

$$\begin{aligned}\nu(k)+N(p) &\rightarrow \nu(k')+\eta(p_{\eta})+N(p')\\ \bar{\nu}(k)+N(p) &\rightarrow \bar{\nu}(k')+\eta(p_{\eta})+N(p'), \qquad N=n,p\end{aligned} \quad (12.41)$$

In the neutral current sector, the structure of current for the non-resonant as well as the resonant contributions, would be similar to that of the charged current ones; however, the form factors would be modified. The form factors for the neutral current induced processes, in the case of non-resonant background terms, are discussed in Section 12.2.2 while the neutral current form factors for the resonance excitations are presented in Chapter 11.

However in this case, there would be additional contribution from the additional isoscalar form factors, arising due to the strangeness component in the nucleon. We will not discuss this subject in this book; the reader is referred to the work of Nieves et al. and the references cited there [481].

https://doi.org/10.1017/9781108489065.013 Published online by Cambridge University Press

12.3.3 Cross section

Figure 12.5 shows the results for the total scattering cross sections for the processes $\nu_\mu + n \longrightarrow \mu^- + \eta + p$ and $\bar{\nu}_\mu + p \longrightarrow \mu^+ + \eta + n$. The individual contributions from the nucleon pole (Born terms), $S_{11}(1535)$ and $S_{11}(1650)$ resonance excitations, where both direct and crossed diagrams are considered, as well as the full model (sum of all the diagrams) are shown. It may be observed from the figure that $S_{11}(1535)$ has the dominant contribution in both the channels and overestimates the full model by $\sim 45\%$. Since the individual contributions of the nucleon pole and $S_{11}(1650)$ are very small as compared to the full model, while depicting the individual contributions, we have scaled them by a factor of 5 and 10 for the process $\nu_\mu + n \longrightarrow \mu^- + \eta + p$ and $\bar{\nu}_\mu + p \longrightarrow \mu^+ + \eta + n$, respectively, in the case of nucleon pole and by a factor of 5 in the case of $S_{11}(1650)$ for both the processes.

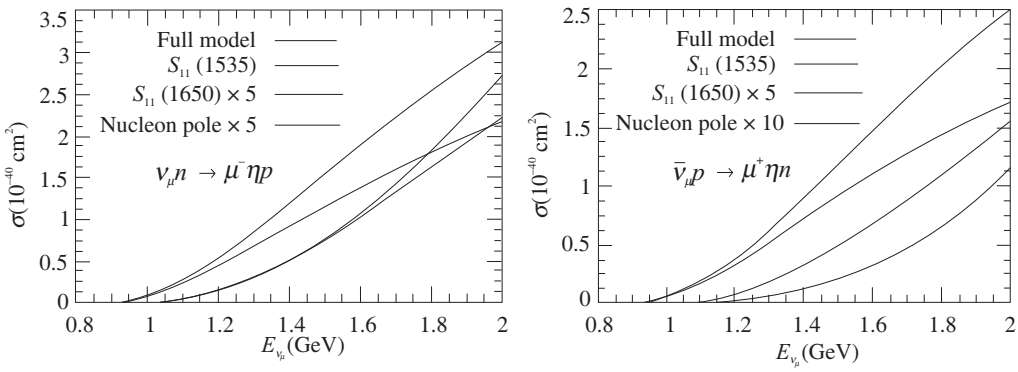

Figure 12.5 Total scattering cross section for the charged current η meson production for the processes $\nu_\mu + n \longrightarrow \mu^- + \eta + p$ and $\bar{\nu}_\mu + p \longrightarrow \mu^+ + \eta + n$. The full model consists of contributions from all the diagrams including $S_{11}(1535)$ and $S_{11}(1650)$. While showing the contribution of the Born terms, $S_{11}(1535)$ and $S_{11}(1650)$, we have taken both direct and cross diagrams. Note that, in order to present on the same scale, $S_{11}(1650)$ and nucleon Born terms are multiplied by 5 for $\nu_\mu n \rightarrow \mu^- \eta p$; for $\bar{\nu}_\mu p \rightarrow \mu^+ \eta n$, the factors are 5 and 10, respectively.

12.4 Associated Production of Strange Particles

The study of the neutrino induced $\Delta S = 0$ associated particle production processes provide an improved understanding of the basic symmetries of the standard model, the structure of the weak hadronic form factors, the strange–quark content of the nucleon, coupling constants, etc. Moreover, the kaon production through the associated production also constitutes a background in the proton decay searches, that is, $p \rightarrow K\bar{\nu}$. Therefore, an understanding and reliable estimate of the cross sections for the neutrino induced kaon production contributing as the background event is important and has been emphasized [526, 527].

The experimental observations of the neutrino induced associated particle production processes were performed earlier at BNL [528], ANL [529], and CERN[530, 453, 452]; however, these experiments have both low statistics and large systematic errors. Attempts are being made to study them in the context of the present-day neutrino experiments with high intensity $\nu(\bar{\nu})$ beams.

https://doi.org/10.1017/9781108489065.013 Published online by Cambridge University Press

Theoretically, early attempts to calculate weak associated production were made by Shrock et al. [531], Mecklenburg et al. [532], Dewan et al. [533], and Amer et al. [534]. The associated particle production cross sections used, for example, in the NUANCE Monte Carlo generator [535] considers only the resonant kaon production based on the Rein and Sehgal model for the pion production [492]. Moreover, these cross sections miss the experimental data points by almost a factor of four [536]. Therefore, a better estimation of the weak interaction induced associated particle production cross section is needed.

Here, the formalism for writing the hadronic current is the same as adopted in the case of pion and eta meson production processes discussed in Sections 12.2 and 12.3, respectively. The CC induced $\Delta S = 0$ processes are the following:

$$\begin{aligned}
\nu_l(k) + p(p) &\longrightarrow l^-(k') + \Sigma^+(p') + K^+(p_k),\\
\nu_l(k) + n(p) &\longrightarrow l^-(k') + \Lambda(p') + K^+(p_k),\\
\nu_l(k) + n(p) &\longrightarrow l^-(k') + \Sigma^0(p') + K^+(p_k),\\
\nu_l(k) + n(p) &\longrightarrow l^-(k') + \Sigma^+(p') + K^0(p_k),\\
\bar{\nu}_l(k) + p(p) &\longrightarrow l^+(k') + \Lambda(p') + K^0(p_k),\\
\bar{\nu}_l(k) + p(p) &\longrightarrow l^+(k') + \Sigma^0(p') + K^0(p_k),\\
\bar{\nu}_l(k) + p(p) &\longrightarrow l^+(k') + \Sigma^-(p') + K^+(p_k),\\
\bar{\nu}_l(k) + n(p) &\longrightarrow l^+(k') + \Sigma^-(p') + K^0(p_k).
\end{aligned} \tag{12.42}$$

The neutral current processes are the following

$$\begin{aligned}
\nu_l/\bar{\nu}_l(k) + p(p) &\longrightarrow \nu_l/\bar{\nu}_l(k') + \Lambda(p') + K^+(p_k),\\
\nu_l/\bar{\nu}_l(k) + p(p) &\longrightarrow \nu_l/\bar{\nu}_l(k') + \Sigma^0(p') + K^+(p_k),\\
\nu_l/\bar{\nu}_l(k) + p(p) &\longrightarrow \nu_l/\bar{\nu}_l(k') + \Sigma^+(p') + K^0(p_k),\\
\nu_l/\bar{\nu}_l(k) + n(p) &\longrightarrow \nu_l/\bar{\nu}_l(k') + \Lambda(p') + K^0(p_K),\\
\nu_l/\bar{\nu}_l(k) + n(p) &\longrightarrow \nu_l/\bar{\nu}_l(k') + \Sigma^0(p') + K^0(p_K),\\
\nu_l/\bar{\nu}_l(k) + n(p) &\longrightarrow \nu_l/\bar{\nu}_l(k') + \Sigma^-(p') + K^+(p_K),
\end{aligned} \tag{12.43}$$

where $l = e, \mu$. For energies above 1.5 GeV, it is the $\Delta S = 0$ kaon production which is more dominant in comparison to the corresponding $|\Delta S| = 1$ processes as the latter is suppressed by a factor of $\tan^2\theta_C$. However, in the case of the antikaon, the $\Delta S = 0$ mode is not possible in the three-body final state due to the change in the total strangeness quantum number by 2 units ($|\Delta S| = 2$). The only possible strangeness conserving process for $K^-, \bar{K}^0$ is through channels like,

$$\nu_l + N \to l^- + K + \bar{K} + N', \qquad (\Delta S = 0). \tag{12.44}$$

However, the threshold for such type of processes is high around 1.6 GeV.

For demonstrating the results of the associated particle production, we have considered only non-resonant diagrams. However, various spin $1/2$ and $3/2$ resonances having an appreciable branching ratio for decays in the KY channel may be included, following the same procedure as

https://doi.org/10.1017/9781108489065.013 Published online by Cambridge University Press

in the case of pion and eta production processes. In Section 12.4.1, we describe the formalism in brief for the charged current induced associated particle production and in Section 12.4.2, the results are presented.

12.4.1 Charged current

The differential scattering cross section for the processes given in Eq. (12.42) is given in Eq. (12.3) with $E_m = E_k$ and $\vec{p}_m = \vec{p}_k$, the outgoing kaon's energy and the three-momentum, respectively. E'_p is replaced with E_Y, the energy of the outgoing hyperon. The transition matrix element for the associated particle production process is given in Eq. (12.4) with the leptonic current defined in Eq. (12.5). The contribution to the hadronic current J^μ comes from the different pieces of the Lagrangian corresponding to the Feynman diagrams shown in Figure 12.6.

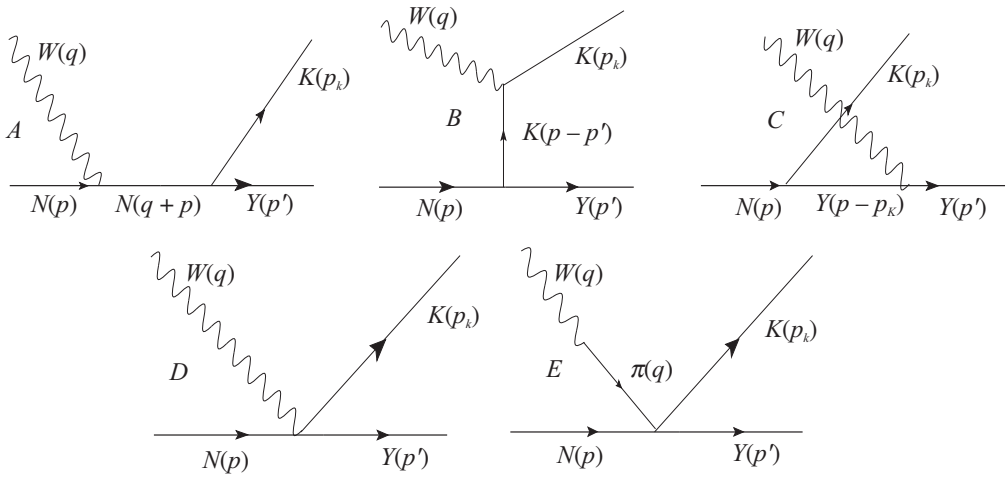

Figure 12.6 Feynman diagrams corresponding to the (anti)neutrino induced $\Delta S = 0$ associated particle production processes.

The matrix element corresponding to the nucleon–hyperon transition may be written as

$$J^\mu = \langle Y(p')|V^\mu - A^\mu|N(p)\rangle. \tag{12.45}$$

The currents V^μ and A^μ are expressed in terms of the vector $f_i(q^2)$ and axial vector $g_i(q^2)$ $N - Y$ transition form factors as [294],

$$V^\mu = \gamma^\mu f_1(q^2) + i\sigma^{\mu\nu}\frac{q^\nu}{M + M_Y} f_2(q^2) + f_3(q^2)\frac{2q^\mu}{M + M_Y}, \tag{12.46}$$

$$A^\mu = \left[\gamma^\mu g_1(q^2) + i\sigma^{\mu\nu}\frac{q^\nu}{M + M_Y} g_2(q^2) + g_3(q^2)\frac{2q^\mu}{M + M_Y}\right]\gamma^5. \tag{12.47}$$

In the vector sector, following the CVC hypothesis, $f_3(q^2) = 0$ and the form factors $f_{1,2}(q^2)$ are determined in terms of the electromagnetic form factors of protons and neutrons, viz.,

https://doi.org/10.1017/9781108489065.013 Published online by Cambridge University Press

$F_{1,2}^{p,n}(q^2)$, as discussed in Chapter 10. The weak electric form factor $g_2(q^2) = 0$ due to G-invariance and SU(3) symmetry.

The axial vector form factor $g_1(q^2)$ comes from the semileptonic hyperon decays and the $\Delta S = 0$ neutrino–nucleon scattering; it is parameterized as

$$g_1(q^2) = g_A(0)\left(1 - \frac{q^2}{M_A^2}\right)^{-2}, \tag{12.48}$$

with axial dipole mass M_A taken as 1.026 GeV.

Applying PCAC, the pseudoscalar transition form factor $(g_3(q^2))$ is related to the axial vector transition form factor $(g_1(q^2))$ as (see Chapter 10 for details)

$$g_3(q^2) = \frac{(M + M_Y)^2}{2(m_K^2 - q^2)} g_1(q^2). \tag{12.49}$$

The form factors $f_{1,2}(q^2)$ in terms of the electromagnetic form factors $F_{1,2}^{p,n}(q^2)$ and $g_1(q^2)$ in terms of the axial vector couplings F and D are listed in Table 12.3. Moreover, we write the amplitudes corresponding to the Feynman diagrams as shown in Figure 12.6 in Eq. (12.50). The various parameters appearing in Eq. (12.50) are tabulated in Table 12.4.

Table 12.3 The standard form factors for weak CC transitions of the SU(3) baryon octet.

Weak transition	$f_1(q^2)$	$f_2(q^2)$	$g_1(q^2)$
$p \to n$	$F_1^p(q^2) - F_1^n(q^2)$	$F_2^p(q^2) - F_2^n(q^2)$	$g_1(q^2)$
$\Sigma^\pm \to \Lambda$	$-\sqrt{\frac{3}{2}} F_1^n(q^2)$	$-\sqrt{\frac{3}{2}} F_2^n(q^2)$	$\sqrt{\frac{2}{3}} \frac{D}{F+D} g_1(q^2)$
$\Sigma^\pm \to \Sigma^0$	$\mp\frac{1}{\sqrt{2}}[2F_1^p(q^2) + F_1^n(q^2)]$	$\mp\frac{1}{\sqrt{2}}[2F_2^p(q^2) + F_2^n(q^2)]$	$\mp\sqrt{2}\frac{F}{F+D} g_1(q^2)$

Table 12.4 Constant factors appearing in the hadronic current. The upper sign corresponds to the processes with antineutrinos and the lower sign to that with neutrinos.

Process	A_{CT}	B_{CT}	A_{SY}	A_{UY}		A_{TY}	A_π
				$Y' = \Sigma$	$Y' = \Lambda$		
$\bar{\nu}_l p \to l^+\Sigma^- K^+$ $\nu_l n \to l^-\Sigma^+ K^0$	0	0	$D - F$	$D - F$	$\frac{1}{3}(D + 3F)$	0	0
$\bar{\nu}_l p \to l^+\Lambda K^0$ $\nu_l n \to l^-\Lambda K^+$	$-\sqrt{\frac{3}{2}}$	$\frac{-1}{3}(D + 3F)$	$\frac{-1}{\sqrt{6}}(D + 3F)$	$-\sqrt{\frac{2}{3}}(D - F)$	0	$\frac{-1}{\sqrt{6}}(D + 3F)$	$\sqrt{\frac{3}{2}}$
$\bar{\nu}_l p \to l^+\Sigma^0 K^0$ $\nu_l n \to l^-\Sigma^0 K^+$	$\mp\frac{1}{\sqrt{2}}$	$D - F$	$\mp\frac{1}{\sqrt{2}}(D - F)$	$\mp\sqrt{2}(D - F)$	0	$\pm\frac{1}{\sqrt{2}}(D - F)$	$\pm\frac{1}{\sqrt{2}}$
$\bar{\nu}_l n \to l^+\Sigma^- K^0$ $\nu_l p \to l^-\Sigma^+ K^+$	-1	$D - F$	0	$F - D$	$\frac{1}{3}(D + 3F)$	$D - F$	1

https://doi.org/10.1017/9781108489065.013 Published online by Cambridge University Press

The hadronic currents corresponding to the diagrams shown in Figure 12.6 now read as

$$\begin{aligned}
j^\mu|_s &= iA_{SY}V_{ud}\frac{\sqrt{2}}{2f_\pi}\,\bar{u}_Y(p')\not{p}_k\gamma^5\frac{\not{p}+\not{q}+M}{(p+q)^2-M^2}\mathcal{H}^\mu u_N(p)\\
j^\mu|_u &= iA_{UY}V_{ud}\frac{\sqrt{2}}{2f_\pi}\,\bar{u}_Y(p')\mathcal{H}^\mu\frac{\not{p}-\not{p}_k+M_Y}{(p-p_k)^2-M_Y}\not{p}_k\gamma^5 u_N(p)\\
j^\mu|_t &= iA_{TY}V_{ud}\frac{\sqrt{2}}{2f_\pi}(M+M_Y)\,\bar{u}_Y(p')\gamma_5\,u_N(p)\;\frac{q^\mu-2p_k^\mu}{(p-p')^2-m_k^2}\\
j^\mu|_{CT} &= iA_{CT}V_{ud}\frac{\sqrt{2}}{2f_\pi}\,\bar{u}_Y(p')\left(\gamma^\mu+B_{CT}\,\gamma^\mu\gamma^5\right)u_N(p)\\
j^\mu|_{\pi F} &= iA_\pi V_{ud}\frac{\sqrt{2}}{4f_\pi}\,\bar{u}_Y(p')(\not{q}+\not{p}_k)u_N(p)\frac{q^\mu}{q^2-m_\pi^2}
\end{aligned}\tag{12.50}$$

where,

$$\mathcal{H}^\mu = f_1(q^2)\gamma^\mu + i\frac{f_2(q^2)}{2M}\sigma^{\mu\nu}q_\nu - g_1(q^2)\left(\gamma^\mu-\frac{\not{q}q^\mu}{q^2-m_\pi^2}\right)\gamma^5 \tag{12.51}$$

is the transition current for $Y \leftrightarrows Y'$ with $Y = Y' \equiv$ nucleon and/or hyperon. Using the expression for hadronic current given in Eq. (12.50), the hadronic tensor $H^{\mu\nu}$ is obtained, which contracts with the leptonic tensor $L^{\mu\nu}$ to get the expression for matrix element squared.

12.4.2 Cross section

The total scattering cross sections for $\nu_\mu N \to \mu^- YK$ and $\bar{\nu}_\mu N \to \mu^+ YK$ processes are shown in Figure 12.7. It may be noted from the figure that the cross section for the reaction with a Λ in the final state are, in general, larger than that for the reactions where a Σ is produced in the final state. This can be understood by looking at the relative strengths of the couplings; for example, the ratio of the square of the couplings for the vertices $nK^0\Lambda$ and $nK^0\Sigma^0$ is $\frac{g^2_{NK\Lambda}}{g^2_{NK\Sigma}} \simeq 14$. Furthermore, the cross section for the Λ production is favoured by the available phase space due to its small mass relative to Σ. Comparing the results of the cross sections for the processes $\nu_\mu p \to \mu^-\Sigma^+K^+$ and $\nu_\mu n \to \mu^-\Lambda K^+$, it is observed that the cross section for the $K^+\Sigma^+$ channel is $\sim 70\%$ smaller at $E_\nu = 1.5$ GeV and $\sim 25\%$ smaller at $E_\nu = 2$ GeV in comparison to the cross section obtained for the $K^+\Lambda$ channel. While the cross sections for the other two channels, viz., $\nu_\mu n \to \mu^-\Sigma^+K^0$ and $\mu^-\Sigma^0K^+$ are much smaller than the cross section for the $K^+\Lambda$ production.

In antineutrino induced processes, it may be noticed that unlike the neutrino induced processes, the channel with Λ in the final state is not very dominating. We find that at low energies, say $E_{\bar{\nu}_\mu} \sim 1.5$ GeV, the cross section for $\bar{\nu}_\mu p \to \mu^+K^0\Lambda$ is around 55% larger than the cross section for $\bar{\nu}_\mu n \to \mu^+K^0\Sigma^-$, while around 2 GeV, the production cross section for $\bar{\nu}_\mu p \to \mu^+K^0\Lambda$ is comparable with that of $\bar{\nu}_\mu n \to \mu^+K^0\Sigma^-$. The cross section for the reaction $\bar{\nu}_\mu p \to \mu^+K^0\Sigma^0$ is around 40% smaller than the cross section for the $K^0\Lambda$ channel at $E_{\bar{\nu}_\mu} = 2$

https://doi.org/10.1017/9781108489065.013 Published online by Cambridge University Press

GeV; whereas, $\bar{\nu}_\mu p \to \mu^+ K^+ \Sigma^-$ cross section is about 10% to the cross section of the $K^0\Lambda$ channel.

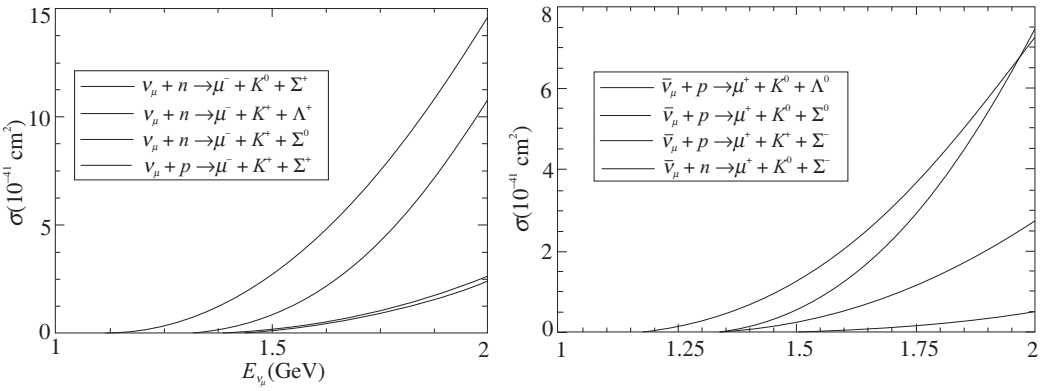

Figure 12.7 Cross section for neutrino (left) and antineutrino (right) induced $|\Delta S| = 0$ associated kaon production processes.

12.5 Kaon Production

In the few GeV energy region, single kaon production processes become important. In principle, their cross sections are smaller than the pionic processes because of the phase space and the Cabibbo suppression for the $\Delta S = 1$ reactions. Nonetheless, in the coming years of precision neutrino physics, their knowledge could be relevant for data analysis, apart from their own intrinsic value related to the role played by strange quarks in hadron physics; in fact, the process is considered a prospective candidate in proton decay searches.

In neutrino induced reactions, the first inelastic reaction creating a strange quark, without accompanying hyperons, is the single kaon production while for antineutrinos, the lowest threshold for $|\Delta S| = 1$ reactions is much lower and corresponds to the hyperon production. This CC $\Delta S = 1$ process is particularly appealing for several reasons. One of them is the better simulation of the background which is produced by atmospheric neutrino interactions in the analysis of one of the main decay channels of the proton, discussed in many SUSY GUT models, that is, $p \to \nu + K^+$ [527, 537, 538]. A second reason is its simplicity from a theoretical point of view. At low energies, it is possible to obtain model independent predictions using the non-linear sigma model and due to the absence of $S = +1$ baryonic resonances, the range of validity of the calculation could be extended to higher energies than for other channels. Furthermore, the associated production of kaons has a higher energy threshold than the single kaon production (1.10 GeV vs. 0.79 GeV). This implies that in the threshold region of associated production, the single kaon production could still be dominant in this energy region of $E_\nu \sim 0.8 - 1.2$ GeV. The basic reaction for the neutrino induced charged current kaon production is

$$\begin{aligned} \nu_l(k) + n(p) &\longrightarrow l^-(k') + n(p') + K^+(p_k), \\ \nu_l(k) + p(p) &\longrightarrow l^-(k') + p(p') + K^+(p_k), \end{aligned}$$

https://doi.org/10.1017/9781108489065.013 Published online by Cambridge University Press

$$\nu_l(k) + n(p) \quad \longrightarrow \quad l^-(k') + p(p') + K^0(p_k), \tag{12.52}$$

where $l = e, \mu$. The expression for the differential scattering cross section in the laboratory frame for this process is given in Eq. (12.3) with $E_m = E_k$ and $\vec{p}_m = \vec{p}_k$, respectively, the energy and three-momentum of the outgoing kaon. The transition matrix element for the single kaon production for the $\Delta S = 1$ process is given as

$$\mathcal{M} = \frac{G_F}{\sqrt{2}} \sin\theta_C \, l_\mu j^\mu, \tag{12.53}$$

with the leptonic current l_μ given in Eq. (12.5).

In the non-resonant sector, four different channels, viz., contact term (CT), kaon pole (KP) term, Σ or Λ hyperon exchanged in the u channel and a meson (π, η) exchange term, may contribute to the hadronic current [490] and are depicted in Figure 12.8. For the single kaon production channel, there is no s channel contribution due to the absence of $S = +1$ baryonic resonances. The current, in the case of the KP term, is proportional to q^μ, which implies that, after contraction with the leptonic tensor, the amplitude is proportional to the lepton mass and therefore, is very small.

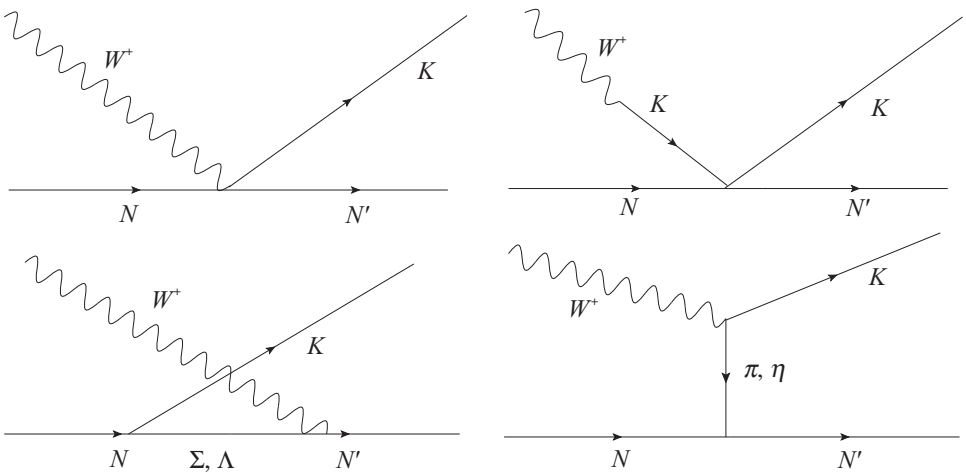

Figure 12.8 Feynman diagrams for the process $\nu N \to l N' K$. The first row from left to right: contact term (labeled CT in the text), kaon pole term (KP); second row: u channel diagram ($C\Sigma$, $C\Lambda$) and pion (eta) in flight (πP, ηP).

In analogy with the single pion production induced by neutrinos [481], as discussed earlier, the different diagrams of Figure 12.8 have the following contributions to the hadronic current:

$$\begin{aligned}
j^\mu\big|_{CT} &= -iA_{CT}\frac{\sqrt{2}}{2f_\pi}\bar{u}(p')(\gamma^\mu + \gamma^\mu\gamma^5 B_{CT})u(p), \\
j^\mu\big|_{C\Sigma} &= iA_{C\Sigma}\frac{\sqrt{2}}{2f_\pi}\bar{u}(p')\left(\gamma^\mu + i\frac{\mu_p + 2\mu_n}{2M}\sigma^{\mu\nu}q_\nu + (D-F)\left(\gamma^\mu - \frac{q^\mu}{q^2 - M_k^2}\not{q}\right)\gamma^5\right) \\
&\quad \times \frac{\not{p} - \not{p}_k + M_\Sigma}{(p-p_k)^2 - M_\Sigma^2}\not{p}_k\gamma^5 u(p),
\end{aligned}$$

https://doi.org/10.1017/9781108489065.013 Published online by Cambridge University Press

$$
\begin{aligned}
j^{\mu}|_{C\Lambda} &= iA_{C\Lambda}\frac{\sqrt{2}}{4f_{\pi}}\bar{u}(p')\left(\gamma^{\mu}+i\frac{\mu_p}{2M}\sigma^{\mu\nu}q_{\nu}-\frac{D+3F}{3}\left(\gamma^{\mu}-\frac{q^{\mu}}{q^2-M_k^2}\not{q}\right)\gamma^5\right)\\
&\quad\times\frac{\not{p}-\not{p}_k+M_{\Lambda}}{(p-p_k)^2-M_{\Lambda}^2}\not{p}_k\gamma^5 u(p),\\
j^{\mu}|_{KP} &= iA_{KP}\frac{\sqrt{2}}{4f_{\pi}}\bar{u}(p')(\not{q}+\not{p}_k)u(p)\frac{1}{q^2-M_k^2}q^{\mu},\\
j^{\mu}|_{\pi} &= iA_{\pi P}(D+F)\frac{\sqrt{2}}{2f_{\pi}}\frac{M}{(q-p_k)^2-M_{\pi}^2}\bar{u}(p')\gamma^5(q^{\mu}-2{p_k}^{\mu})u(p),\\
j^{\mu}|_{\eta} &= iA_{\eta P}(D-3F)\frac{\sqrt{2}}{2f_{\pi}}\frac{M}{(q-p_k)^2-M_{\eta}^2}\bar{u}(p')\gamma^5(q^{\mu}-2{p_k}^{\mu})u(p),
\end{aligned}
\tag{12.54}
$$

where, $q = k - k'$ is the four-momentum transfer, $\mu_p = 1.7928\ \mu_N$, and $\mu_n = -1.9130\ \mu_N$ are, respectively, the proton and neutron anomalous magnetic moments. The value of the various parameters appearing in the expressions of the hadronic currents of the different channels are shown in Table 12.5. If the cross sections for the single kaon processes were measured with some precision, one could use them to explore these form factors at several q^2 values. The current experimental information, based on semileptonic decays, covers only a very reduced range for this magnitude.

Table 12.5 Values of the parameters appearing in the hadronic currents.

Process	A_{CT}	B_{CT}	$A_{C\Sigma}$	$A_{C\Lambda}$	A_{KP}	$A_{\pi P}$	$A_{\eta P}$
$\nu_l + n \to l^- + K^+ + n$	1	$D-F$	$-(D-F)$	0	1	1	1
$\nu_l + p \to l^- + K^+ + p$	2	$-F$	$-(D-F)/2$	$(D+3F)$	2	-1	1
$\nu_l + n \to l^- + K^0 + p$	1	$-(D+F)$	$(D-F)/2$	$(D+3F)$	1	-2	0

These processes are least studied experimentally; thus, the information regarding the q^2 dependence of $D(q^2)$ and $F(q^2)$ in Eq. (12.54) are not known. To incorporate the hadronic structure in the matrix element, a dipole form factor

$$F(q^2) = 1/(1 - q^2/M_F^2)^2, \tag{12.55}$$

is used with a mass $M_F \simeq 1$ GeV. Its effect, being small at low neutrino energies, will give an idea of the uncertainties of the calculation which is explored in the next section.

However, recently the MINERvA experiment [539] has measured the differential scattering cross section for the charged current induced single kaon production as a function of the kinetic energy of the kaon produced in the final state.

12.5.1 Cross section

Figure 12.9 shows the results of the contributions of the different diagrams to the total scattering cross sections for the processes $\nu_\mu p \longrightarrow \mu^- K^+ p$ and $\nu_\mu n \to \mu^- K^0 p$. It may be observed

https://doi.org/10.1017/9781108489065.013 Published online by Cambridge University Press

that the contact term has a dominant contribution to the total scattering cross section in both the processes studied. The curve labeled as the full model is calculated with a dipole form factor with $M_F = 1$ GeV. The band corresponds to the variation of M_F by 10%. The process $\nu_\mu + n \to \mu^- + K^0 + p$ has a cross section of a similar size and the contact term is the largest followed by the π exchange diagram and the u channel (Λ) term. The rate of increase of the cross sections for the process $\nu_\mu n \to \mu^- p K^0$ is larger and could become more important at higher energies. We observe a destructive interference between the different terms; the cross section obtained with the full model is smaller than that produced by the contact term.

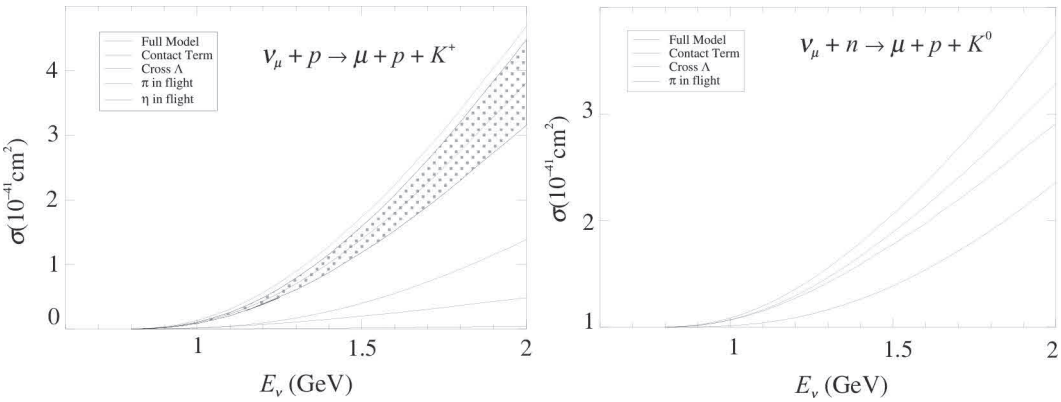

Figure 12.9 Contribution of the different terms to the total scattering cross section for the $\nu_\mu + p \longrightarrow \mu^- + K^+ + p$ (left panel) and $\nu_\mu + n \longrightarrow \mu^- + K^0 + p$ (right panel) processes.

It must be noted that due to the higher threshold of the associated kaon production, the reactions we have studied are the dominant source of kaons for a wide range of energies, and thus, their study is important for lower energy accelerator experiments as well as for atmospheric neutrino experiments.

12.6 Antikaon Production

We have seen earlier that the hyperon and kaon productions ($|\Delta S| = 1$) are important in the few GeV energy region, although they are small due to the Cabibbo suppression. In this section, we describe the weak single antikaon production off the nucleons in the charged current sector induced by antineutrinos. Other processes like the charged current induced neutrino processes as well as the neutral current induced neutrino and antineutrino processes are forbidden by the $\Delta S \neq \Delta Q$ rule. The resonant excitations, absent for the kaon case, also contribute to the single antikaon production.

The basic reaction for the antineutrino induced charged current antikaon production is

$$\begin{aligned} \bar{\nu}_l(k) + p(p) &\longrightarrow l^+(k') + p(p') + K^-(p_k), \\ \bar{\nu}_l(k) + n(p) &\longrightarrow l^+(k') + n(p') + K^-(p_k), \\ \bar{\nu}_l(k) + p(p) &\longrightarrow l^+(k') + n(p') + \bar{K}^0(p_k), \end{aligned} \tag{12.56}$$

https://doi.org/10.1017/9781108489065.013 Published online by Cambridge University Press

where $l = e, \mu$; the quantities in the parentheses represent the four-momenta of the corresponding particles.

The expression for the differential scattering cross section is given in Eq. (12.3), where $E_m = E_k$ is the energy of the outgoing antikaon and $\vec{p}_m = \vec{p}_k$ represents the three-momentum of the antikaon. The transition matrix element is defined in Eq. (12.53) with the leptonic current given in Eq. (12.5). The hadronic current receives the contribution from the non-resonant background terms as well as from the decuplet resonance terms, presented in Figure 12.10. The non-resonant as well as the decuplet resonance terms are obtained using the non-linear sigma model. The different channels which contribute to the hadronic currents are the s channel with Σ, Λ(SC), and Σ^*(SCR) as the intermediate states, the kaon pole (KP) term, contact term (CT), and meson (πP,ηP) exchange term [491]. For the single antikaon processes, there are no u channel processes with the hyperons in the intermediate state.

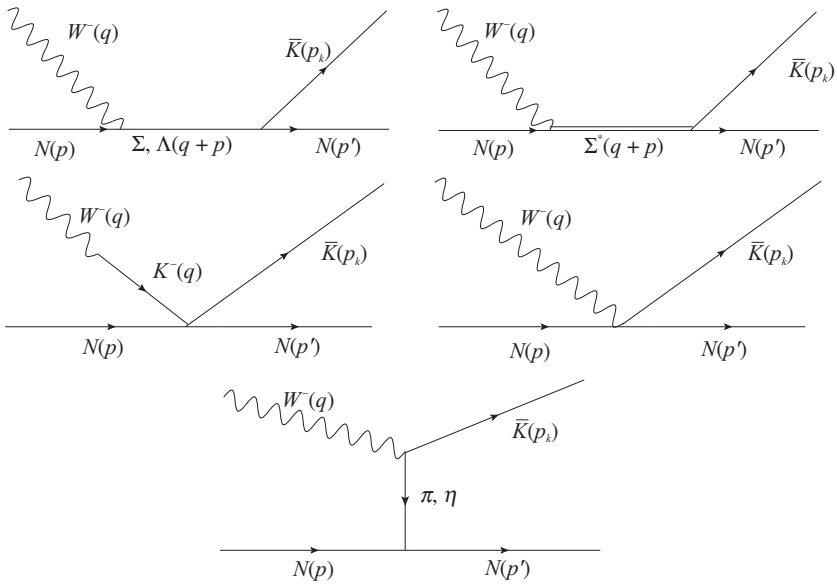

Figure 12.10 Feynman diagrams for the process $\bar{\nu}N \to lN'\bar{K}$. The first row from left to right: s channel Σ, Λ propagator (labeled SC in the text), s channel Σ^* resonance (SCR); second row: kaon pole term (KP); contact term (CT) and last row: pion(Eta) in flight ($\pi P/\eta P$).

As in the case of the pion production where $P_{33}(1232)$ contributes significantly, the excitation of $\Sigma^*(1385)$ resonance and its subsequent decay in $N\bar{K}$ may be important in the single antikaon production processes. The lowest order SU(3) Lagrangian for the coupling of the pseudoscalar mesons with the decuplet–octet baryons, in the presence of the external weak current, is given by [540]

$$\mathcal{L}_{dec} = \mathcal{C}\left(\epsilon^{abc}\bar{T}^{\mu}_{ade}u^{d}_{\mu,b}B^{e}_{c} + h.c.\right), \tag{12.57}$$

where T^{μ} is the SU(3) representation of the decuplet fields,

https://doi.org/10.1017/9781108489065.013 Published online by Cambridge University Press

$$T_{ijk} = \begin{pmatrix} \Delta^{++} & \frac{1}{\sqrt{3}}\Delta^{+} & \frac{1}{\sqrt{3}}\Sigma^{*+} \\ \frac{1}{\sqrt{3}}\Delta^{+} & \frac{1}{\sqrt{3}}\Delta^{0} & \frac{1}{\sqrt{6}}\Sigma^{*0} \\ \frac{1}{\sqrt{3}}\Sigma^{*+} & \frac{1}{\sqrt{6}}\Sigma^{*0} & \frac{1}{\sqrt{3}}\Xi^{*0} \end{pmatrix} \begin{pmatrix} \frac{1}{\sqrt{3}}\Delta^{+} & \frac{1}{\sqrt{3}}\Delta^{0} & \frac{1}{\sqrt{6}}\Sigma^{*0} \\ \frac{1}{\sqrt{3}}\Delta^{0} & \Delta^{-} & \frac{1}{\sqrt{3}}\Sigma^{*-} \\ \frac{1}{\sqrt{6}}\Sigma^{*0} & \frac{1}{\sqrt{3}}\Sigma^{*-} & \frac{1}{\sqrt{3}}\Xi^{*-} \end{pmatrix} \begin{pmatrix} \frac{1}{\sqrt{3}}\Sigma^{*+} & \frac{1}{\sqrt{6}}\Sigma^{*0} & \frac{1}{\sqrt{3}}\Xi^{*0} \\ \frac{1}{\sqrt{6}}\Sigma^{*0} & \frac{1}{\sqrt{3}}\Sigma^{*-} & \frac{1}{\sqrt{3}}\Xi^{*-} \\ \frac{1}{\sqrt{3}}\Xi^{*0} & \frac{1}{\sqrt{3}}\Xi^{*-} & \Omega^{-} \end{pmatrix}, \tag{12.58}$$

$a - e$ are flavor indices, B corresponds to the baryon octet, and u_μ is the SU(3) representation of the pseudoscalar mesons interacting with weak left l_μ and right r_μ handed currents, discussed in Chapter 11. The different physical states of the decuplet corresponding to T_{ijk} are given in Table 12.6. The parameter $\mathcal{C} \simeq 1$ is fitted to the $\Delta(1232)$ decay width. The spin 3/2 propagator for Σ^* is given by

Table 12.6 The physical states of the decuplet .

T_{111}	Δ^{++}	T_{112}	$\frac{\Delta^{+}}{\sqrt{3}}$	T_{113}	$\frac{\Sigma^{*+}}{\sqrt{3}}$	T_{123}	$\frac{\Sigma^{*0}}{\sqrt{6}}$	T_{233}	$\frac{\Xi^{-}}{\sqrt{3}}$
T_{122}	$\frac{\Delta^{0}}{\sqrt{3}}$	T_{222}	Δ^{-}	T_{223}	$\frac{\Sigma^{*-}}{\sqrt{3}}$	T_{133}	$\frac{\Xi^{0}}{\sqrt{3}}$	T_{333}	Ω^{-}

$$G^{\mu\nu}(P) = \frac{P^{\mu\nu}_{RS}(P)}{P^2 - M^2_{\Sigma^*} + iM_{\Sigma^*}\Gamma_{\Sigma^*}}, \tag{12.59}$$

where $P = p + q$ is the momentum carried by the resonance and $P^{\mu\nu}_{RS}$ is the projection operator for the spin 3/2 resonances, given as

$$P^{\mu\nu}_{RS}(P) = \sum_{\text{spin}} \psi^\mu \bar{\psi}^\nu = -(\not{P} + M_{\Sigma^*}) \left[g^{\mu\nu} - \frac{1}{3}\gamma^\mu\gamma^\nu - \frac{2}{3}\frac{P^\mu P^\nu}{M^2_{\Sigma^*}} + \frac{1}{3}\frac{P^\mu\gamma^\nu - P^\nu\gamma^\mu}{M_{\Sigma^*}} \right], \tag{12.60}$$

with M_{Σ^*} the resonance mass and ψ^μ, the Rarita–Schwinger spinor. The decay width of Σ^*, obtained using the Lagrangian given in Eq. (12.57), can be written as

$$\Gamma_{\Sigma^*} = \Gamma_{\Sigma^* \to \Lambda\pi} + \Gamma_{\Sigma^* \to \Sigma\pi} + \Gamma_{\Sigma^* \to N\bar{K}}, \tag{12.61}$$

where

$$\Gamma_{\Sigma^* \to Y,\,\text{meson}} = \frac{C_Y}{192\pi}\left(\frac{\mathcal{C}}{f_\pi}\right)^2 \frac{(W + M_Y)^2 - m^2}{W^5} \lambda^{3/2}(W^2, M_Y^2, m^2)\,\Theta(W - M_Y - m). \tag{12.62}$$

https://doi.org/10.1017/9781108489065.013 Published online by Cambridge University Press

Here, m, M_Y are the masses of the emitted meson and baryon, $\lambda(x,y,z) = (x-y-z)^2 - 4yz$ and Θ is the step function. The factor C_Y is 1 for Λ and $\frac{2}{3}$ for N and Σ.

Using the symmetry arguments, we may write the most general $W^- N \to \Sigma^*$ vertex in terms of a vector and an axial vector part as

$$\langle \Sigma^*; P = p+q\,|V^\mu|N;p\rangle = \sin\theta_C \bar{\psi}_\alpha(\vec{P})\Gamma_V^{\alpha\mu}(p,q)\,u(\vec{p}\,), \tag{12.63}$$

$$\langle \Sigma^*; P = p+q\,|A^\mu|N;p\rangle = \sin\theta_C \bar{\psi}_\alpha(\vec{P})\Gamma_A^{\alpha\mu}(p,q)\,u(\vec{p}\,), \tag{12.64}$$

where

$$\begin{aligned}\Gamma_V^{\alpha\mu}(p,q) &= \left[\frac{C_3^V}{M}\left(g^{\alpha\mu}\not{q} - q^\alpha\gamma^\mu\right) + \frac{C_4^V}{M^2}\left(g^{\alpha\mu}q\cdot P - q^\alpha P^\mu\right) + \frac{C_5^V}{M^2}\left(g^{\alpha\mu}q\cdot p - q^\alpha p^\mu\right)\right.\\ &\qquad \left. + C_6^V g^{\mu\alpha}\right]\gamma_5\\ \Gamma_A^{\alpha\mu}(p,q) &= -\left[\frac{C_3^A}{M}\left(g^{\alpha\mu}\not{q} - q^\alpha\gamma^\mu\right) + \frac{C_4^A}{M^2}\left(g^{\alpha\mu}q\cdot P - q^\alpha P^\mu\right) + C_5^A g^{\alpha\mu} + \frac{C_6^A}{M^2}q^\mu q^\alpha\right].\end{aligned} \tag{12.65}$$

Our knowledge of these form factors is quite limited. The Lagrangian given in Eq. (12.57) gives only $C_5^A(0) = -2\mathcal{C}/\sqrt{3}$ (for the $\Sigma^{*-}(1385)$ case). However, using the SU(3) symmetry, all the other form factors of $\Sigma^{*-}(1385)$ may be related to the corresponding form factors of the $\Delta(1232)$ resonance, such that $C_i^{\Sigma^{*-}}/C_i^{\Delta^+} = -1$ and $C_i^{\Sigma^{*-}}/C_i^{\Sigma^{*0}} = \sqrt{2}$. In the case of the Δ resonance, as discussed in Section 12.2, the weak vector form factors are relatively known from the electromagnetic processes and there is some information on the axial vector form factors from the study of the pion production. The vector form factors for the Δ resonances, discussed in Chapter 11, are used while the axial vector form factors $C_5^A(q^2)$ is determined from the decay width of the resonances in the pionic channels; $C_6^A(q^2)$ is determined using PCAC.

The hadronic currents for the background and resonant terms are written as

$$\begin{aligned}J^\mu|_{CT} &= iA_{CT}V_{us}\frac{\sqrt{2}}{2f_\pi}\bar{u}(p')\left(\gamma^\mu + B_{CT}\,\gamma^\mu\gamma_5\right)u(p)\\ J^\mu|_{\Sigma} &= iA_\Sigma(D-F)V_{us}\frac{\sqrt{2}}{2f_\pi}\bar{u}(p')\not{p}_k\gamma_5\frac{\not{p}+\not{q}+M_\Sigma}{(p+q)^2-M_\Sigma^2}\left(\gamma^\mu + i\frac{(\mu_p+2\mu_n)}{2M}\sigma^{\mu\nu}q_\nu\right.\\ &+ \left.(D-F)\left\{\gamma^\mu - \frac{q^\mu}{q^2-{M_k}^2}\not{q}\right\}\gamma^5\right)u(p)\\ J^\mu|_{\Lambda} &= iA_\Lambda V_{us}(D+3F)\frac{1}{2\sqrt{2}f_\pi}\bar{u}(p')\not{p}_k\gamma^5\frac{\not{p}+\not{q}+M_\Lambda}{(p+q)^2-M_\Lambda^2}\left(\gamma^\mu + i\frac{\mu_p}{2M}\sigma^{\mu\nu}q_\nu\right.\\ &- \left.\frac{(D+3F)}{3}\left\{\gamma^\mu - \frac{q^\mu}{q^2-{M_k}^2}\not{q}\right\}\gamma^5\right)u(p)\\ J^\mu|_{KP} &= iA_{KP}V_{us}\frac{\sqrt{2}}{2f_\pi}\bar{u}(p')\not{q}\;u(p)\frac{q^\mu}{q^2-M_k^2}\end{aligned}$$

https://doi.org/10.1017/9781108489065.013 Published online by Cambridge University Press

$$
\begin{aligned}
J^{\mu}|_{\pi} &= iA_{\pi}\frac{M\sqrt{2}}{2f_{\pi}}V_{us}(D+F)\frac{2p_k{}^{\mu}-q^{\mu}}{(q-p_k)^2-m_{\pi}{}^2}\bar{u}(p')\gamma_5 u(p) \\
J^{\mu}|_{\eta} &= iA_{\eta}\frac{M\sqrt{2}}{2f_{\pi}}V_{us}(D-3F)\frac{2p_k{}^{\mu}-q^{\mu}}{(q-p_k)^2-m_{\eta}{}^2}\bar{u}(p')\gamma_5 u(p) \\
J^{\mu}|_{\Sigma^*} &= -iA_{\Sigma^*}\frac{\mathcal{C}}{f_{\pi}}\frac{1}{\sqrt{6}}\,V_{us}\,\frac{p_k^{\lambda}}{P^2-M_{\Sigma^*}^2+i\Gamma_{\Sigma^*}M_{\Sigma^*}}\,\bar{u}(p')P_{RS_{\lambda\rho}}(\Gamma_V^{\rho\mu}+\Gamma_A^{\rho\mu})u(p)
\end{aligned}
$$

In $\Gamma_V^{\rho\mu}+\Gamma_A^{\rho\mu}$, the form factors are taken as for the Δ^+ case. The factors A_i for each diagram contributing to the hadronic current are tabulated in Table 12.7.

In analogy with the single kaon production, a global dipole form factor given in Eq. (12.55) with $M_F \simeq 1$ GeV is used in the hadronic currents, except for the resonance excitation.

Table 12.7 Constant factors appearing in the hadronic current.

Process	B_{CT}	A_{CT}	A_{Σ}	A_{Λ}	A_{KP}	A_{π}	A_{η}	A_{Σ^*}
$\bar{\nu}_l + n \to l^+ + K^- + n$	$D-F$	1	-1	0	-1	1	1	2
$\bar{\nu}_l + p \to l^+ + K^- + p$	$-F$	2	$-\frac{1}{2}$	1	-2	-1	1	1
$\bar{\nu}_l + p \to l^+ + \bar{K}^0 + n$	$-(D+F)$	1	$\frac{1}{2}$	1	-1	-2	0	-1

12.6.1 Cross section

In Figure 12.11, the different contributions of the hadronic current to the $\bar{\nu}_\mu p \to \mu^+ pK^-$ and $\bar{\nu}_\mu n \to \mu^+ nK^-$ reactions are presented. It may be observed that the cross section is dominated

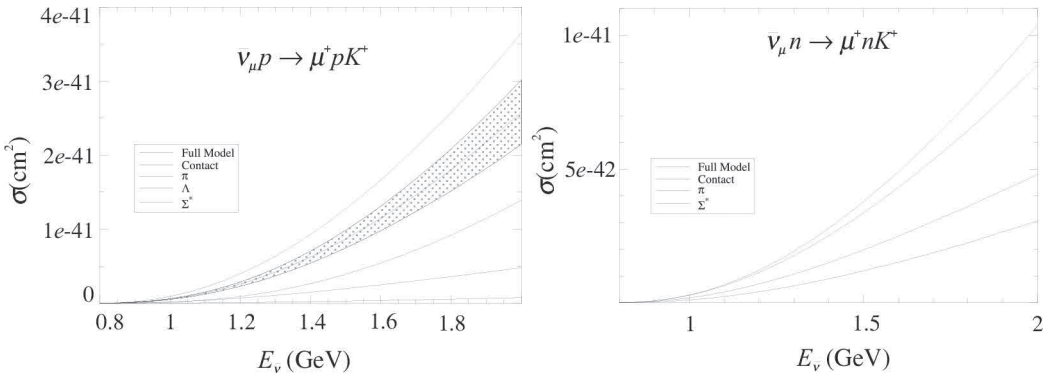

Figure 12.11 Total scattering cross section for the processes $\bar{\nu}_\mu p \to \mu^+ pK^-$ and $\bar{\nu}_\mu n \to \mu^+ nK^-$.

by the non-resonant terms, with contact term providing the largest contribution. Destructive interference leads to a total scattering cross section smaller than that predicted by the CT term. It should be noted that in the case of the $\bar{\nu}_\mu p \to \mu^+ pK^-$ process, $\Sigma^*(1385)$ has negligible contribution. The curve labeled as full model is calculated with a dipole form factor with a

https://doi.org/10.1017/9781108489065.013 Published online by Cambridge University Press

mass of 1 GeV. The band corresponds to a 10% variation in M_F. For the $\bar{\nu}_\mu n \to \mu^+ n K^-$ case, the contribution of Σ^* resonance is substantial due to the larger value of the couplings (see Table 12.7).

https://doi.org/10.1017/9781108489065.013 Published online by Cambridge University Press